Energy-Efficient and Low-Complexity Transmission Control with SWIPT-NOMA for Green Cellular Networks

Thi My Tuyen Nguyen, The Vi Nguyen, Wonjong Noh, *Senior Member, IEEE*, and Sungrae Cho, *Member, IEEE*

***Abstract*—In this study, we consider an energy-efficient and low-complexity transmission control in a SWIPT-NOMA-based green cellular network (GCN) that consists of a green base station (GBS) and green users (GUEs). First, we formulate a non-convex problem that minimizes transmit power consumption while supporting minimum downlink user service rate, downlink data queue stability, and user battery availability. Then, we transform the problem into a Lyapunov-drift-penalty minimization problem, which can determine a new resource allocation scheme that balances transmit power consumption and queue stability. Second, the Lyapunov-drift-penalty problem is decomposed into subchannel assignment, power allocation, and power splitting (PS) ratio control problems. The subchannel assignment problem is solved using a matching theory-based low-complexity algorithm. The power allocation and PS ratio control problems are solved using the alternating optimization (AO) approach and bisection method. This decomposed subproblem-based control also enables distributed control between the GBS and GUEs. Third, we prove the convergence, optimality, and polynomial computation complexity of the proposed algorithm. Lastly, we demonstrate that the proposed control outperforms the benchmark controls regarding transmit power consumption and the achievable rate. Owing to the optimality and low complexity, the proposed control can be efficiently applied to large-scale and distributed GCNs in sixth-generation environments.**

***Index Terms*—Green Cellular Network, Lyapunov Optimization, NOMA, SWIPT, Queue Stability**

I. Introduction

Because of the exponentially increasing internet of things (IoT) devices, designing energy-efficient green communication systems (GCNs) that consist of a green base station (GBS) and green users (GUEs) is increasingly becoming important in upcoming sixth-generation (6G) environments. Some of the representative future GCNs could be unmanned aerial vehicle-based networks, low-earth orbit/geostationary-earth orbit satellite-based networks, underwater networks, and spacecraft networks. These networks are envisioned to support mission-critical applications, autonomous driving, industrial automation, public safety, remote monitoring, and vehicle-to-everything (V2X) communication in network environments where power supply is limited [1].

Several paradigm-shifting technologies, such as nonorthogonal multiple access (NOMA) and simultaneous wireless information and power transfer (SWIPT), must be considered to design energy-efficient green systems. Recently, NOMA technology has been introduced to boost the system capacity over orthogonal multiple access (OMA) systems with restricted resources. Contrary to OMA methods, NOMA can minimize the transmission latency for each user by offering additional access in the power domain. However, because of the design complexity of NOMA, in particular with massive multiple-input multiple-output (MIMO) [2], transitioning from an OMA-GCN to a NOMA-GCN presents many challenges. Second, SWIPT provides a promising solution to energy-constrained networks, such as the IoT networks and wireless sensor networks. In addition, SWIPT allows the energy-constrained node to extract information and energy from the received radio frequency (RF) signals simultaneously. Receiver architectures based on time switching (TS) and power splitting (PS) were proposed to realize the SWIPT [3].

A. Related Works

Recent studies have combined NOMA and SWIPT to prolong the lifetime of the energy-constrained networks and support massive connectivity. Mao *et al.* [4] focused on energy-efficient resource allocation. They adopted a non-linear EH model and proposed a penalty function-based resource allocation algorithm. Song *et al.* [5] suggested a joint power allocation and sensing time optimization algorithm based on a dichotomy method to achieve the optimal resource allocation solution in a NOMA-based SWIPT system. Tang *et al.* [6], [7] investigated joint power allocation and TS or PS controls. They aimed to maximize the total transmission rate and harvested energy considering the maximum transmit power budget, minimum data rate, and minimum harvested energy per terminal. Andrawes *et al.* [8] optimized power allocation and PS to maximize energy efficiency under the eligible spectral efficiency using the genetic algorithm. The outage probability for the near and far users was considered for the optimization process. Diamantoulakis *et al.* [9] investigated proportional fairness maximization among users in uplink NOMA-SWIPT. In particular, some studies [10]–[12] have investigated the secrecy sum-rate optimization problem for SWIPT-enabled NOMA systems.

This research was supported by the MSIT (Ministry of Science and ICT), Korea, under the ITRC (Information Technology Research Center) support program (IITP-2023-RS-2022-00156353) supervised by the IITP (Institute for Information Communications) and National Research Foundation of Korea (NRF) grant (NRF-2020R1F1A1069119). It was also supported by the Chung-Ang University Young Scientist Scholarship in 2021. *(Corresponding authors: Wonjong Noh and Sungrae Cho.)*

T. M. T. Nguyen, T. V. Nguyen, and S. Cho are with the School of Computer Science and Engineering, Chung-Ang University, Seoul 156-756, South Korea (e-mail: tuyen@uclab.re.kr, tvnguyen@uclab.re.kr, srcho@cau.ac.kr).

W. Noh is with the School of Software, Hallym University, Chuncheon 24252, South Korea (e-mail: wonjong.noh@hallym.ac.kr).

Furthermore, cooperative SWIPT-based NOMA has also attracted considerable research interest. In [13], the application of SWIPT to NOMA networks where users are spatially randomly located was investigated. It confirmed that the opportunistic use of node locations for user selection can achieve a low outage probability and deliver superior throughput compared to the random selection scheme. Do *et al.* [14] studied the performance of a cell-edge user in a two-user multiple-input single-output (MISO) NOMA system, where a cell center user acts as a relay to assist the cell-edge user. In addition, its relaying operation is powered by a hybrid TS/PS SWIPT protocol, and transmit antenna selection protocols are employed. Some researchers [15], [16] have considered SWIPT-enabled full-duplexing cooperative NOMA systems. They derived the outage probabilities and ergodic rates of both the near and far users under adaptive and fixed power allocation strategies.

Understanding the influence of hardware impairments and imperfect channel state information (CSI) on the SWIPT-assisted NOMA systems has recently attracted substantial interest [17]. Due to hardware impairments and imperfect CSI, successive interference cancellation (SIC) cannot be error-free. There is residual power from incompletely canceled previous symbols. This SIC error can propagate and increase with a rising number of simultaneously connected users [18]. Guo *et al.* [19] focused on analyzing the combined effect of hardware impairments and imperfect CSI on a SWIPT-assisted adaptive NOMA/OMA system with user selection. In the NOMA mode, the near users employ the PS receiver architecture to harvest energy and act as a decode-and-forward relay to forward the far users' signals. In addition, in the existing wireless communication system, CSI at the transmitter is obtained by feedback links, but the finite-rate uplink cannot precisely receive the instantaneous perfect CSI because of the limited resources and quantization errors. Therefore, Zhou *et al.* [20] employed statistical CSI that can be easily and accurately obtained. Xu *et al.* [21] proposed the imperfect CSI-based energy-efficient resource allocation scheme in NOMA-based device-to-device networks with SWIPT.

Some researchers [22], [23] have considered data-buffer-aided communications in SWIPT-NOMA networks, which has attracted considerable research attention because it opens up a new degree of freedom to improve the system capacity and energy efficiency. However, most previous studies have assumed that the harvested energy could be used immediately within one transmission block, leading to poor performance in terms of long-term power consumption. Therefore, Ren *et al.* [24] formulated a long-term time-average sum-rate maximization problem, guaranteeing the stability of all users' data and energy queues. Then, an online scheduling scheme based on the Lyapunov optimization framework was proposed to solve the long-term stochastic optimization problem. Accordingly, control decisions and resource allocations were performed according to the real-time CSI and buffer states. For the buffer-aided relaying system, the relay can adaptively select the operation mode between the relay reception and relay transmission based on the current CSI, which enables a larger network throughput at the cost of an increased queueing delay. This approach motivated [25], who formulated a long-term time-average power consumption minimization problem considering the data and energy queue causality, peak transmit power constraint, and transmission mode selection. To make the problem easier to be handled, they demonstrated how to transform the long-term time-average power consumption minimization problem into a real-time optimization problem using the Lyapunov optimization framework. On this basis, the buffer-aided adaptive transmission scheme was derived.

B. Motivation and Contribution

To our knowledge, no study has simultaneously considered energy efficiency and queue stability in the non-linear energy harvesting SWIPT-NOMA based GCNs. Therefore, we were motivated to study and develop an energy-efficient and queue-stable SWIPT-NOMA control scheme while satisfying important quality-of-service (QoS) requirements in GCNs. The key aspects of the proposed method and that of the other existing studies are compared in Table I. The main contributions can be summarized as follows:

- In this work, we formulate a non-convex problem that minimizes transmit power consumption while supporting minimum downlink user rate, downlink data queue stability, and user battery availability. Then, we transform the long-term stochastic control problem into a Lyapunov-drift-penalty minimization problem. This approach performs a new resource allocation control through an opportunistic slot-by-slot decision while balancing data and the battery queue stability and power consumption.
- We decompose the problem into subchannel assignment, power allocation, and PS ratio control problems. We solve the subchannel assignment problem using a matching theory-based low-complexity algorithm. The power allocation and PS ratio control problems are solved using an alternating optimization (AO) approach and the bisection method. The decomposed subproblem-based control enables distributed controls between the GBS and GUEs.
- We rigorously prove that the proposed matching theory and AO-based approach stably converges to a nearly-optimal solution and demonstrate that the proposed control has polynomial computation complexity. Owing to the optimality and low complexity of the proposed solution, the proposed controls can be efficiently applied to large-scale and distributed GCNs in 6G environments.
- Through simulations, we demonstrate that the proposed control outperforms benchmark controls regarding transmit power consumption and achievable rate.

The remainder of this paper is organized as follows. Section II introduces the system model and presents the problem formulation. Next, Section III presents a Lyapunov optimization-based problem reformulation and optimization. Section IV proposes the matching theory and AO-based low-complexity solutions for subchannel assignment, power allocation, and PS ratio decisions in the SWIPT-NOMA system. Then, Section V provides numerical results demonstrating the correctness of the proposed control. Finally, conclusions are presented in Section VI.

TABLE I
COMPARISON OF THE PROPOSED AND EXISTING SWIPT-NOMA-BASED STUDIES.

Ref.	System	Optimization objective	EH model	Optimization variables	Optimization methods
[4]	Cognitive-NOMA with SWIPT	System power consumption	Non-linear [(2)]	Transmit beam former, PS control [(4)]	Semi-definite relaxation, SCA [(7)]
[5]	Cognitive-NOMA with SWIPT	Achievable throughput	Linear [(3)]	Power allocation, sensing time	Lagrangian dual method, bisection method
[6]	NOMA-SWIPT	Energy efficiency	Linear	Power allocation, TS control [(5)]	AO algorithm [(8)] Lagrangian dual method
[7]	MC-NOMA with SWIPT	Achievable data rate	Linear	Power allocation, PS control	AO algorithm, Lagrangian dual method, and deep-learning-based method
[24]	WPCN [(1)] with NOMA	Time-average sum rate	Linear	WPT and WIT [(6)] mode selection, arrival rate control, energy beamforming, rate and power allocations	Lyapunov-based online optimization
[25]	Cooperative NOMA-relay with SWIPT	Time average power consumption	Linear	Rate allocation, power allocation, and transmission mode selection	Lyapunov-based online optimization
Proposed	NOMA-SWIPT	Time average power consumption	Non-linear	subchannel assignment, power allocation, and PS control	Lyapunov-based online optimization, AO algorithm, and matching algorithm

[(1)] WPCN: wireless-powered communication network
[(2)] The harvested energy first increases almost linearly as the received power increases, and then saturates as the received power reaches a specific level
[(3)] The harvested energy at the EH receiver is linearly and directly proportional to the received power
[(4), (5)] PS: power splitting and TS: time switching schemes in SWIPT
[(6)] WPT: wireless power transmission and WIT: wireless information transmission
[(7), (8)] SCA: successive convex approximation algorithm and AO: alternating optimization algorithm

II. System Model and Problem Formulation

In this section, we elaborate on the proposed system model in Fig. 1 and problem formulation.

A. Network Model

We consider a single-cell downlink system in which one single-antenna GBS serves $2N$ single-antenna GUEs. We assume that the whole cell region is divided into two regions centered at the GBS: the *inner region* with radius r_i and *outer region* with radius r_o. According to these regions, we assume that users are classified as inner and outer users, respectively. We assume that N inner GUEs and N outer GUEs exist, and the set of GUEs is denoted as $\mathcal{N} \triangleq \{1, \ldots, 2N\}$. The users are assumed to be grouped in pairs of one inner and one outer user. The set of user groups is denoted as $\mathcal{G} \triangleq \{1, 2, \ldots, N\}$. For $g \in \mathcal{G}$, the g-th pair includes an outer user, indexed as $2g-1$, and an inner user, indexed as $2g$. The total bandwidth B is equally divided into M subchannels, denoted by $\mathcal{M} \triangleq \{1, \ldots, M\}$, where $M = N$. The set of time slots is denoted as $\mathcal{T} = \{0, \ldots, t, \ldots, T-1\}$. At each time slot, all GUEs simultaneously receive data and energy from the GBS and send their battery state information and CSI to the serving GBS.

B. SWIPT-NOMA Model

According to the NOMA protocol [26], one subchannel can be allocated to multiple users. However, to reduce the multiple-access interference produced by subchannel sharing among users and decrease the complexity of SIC decoding operations at the receiver side, we consider that each subchannel can be assigned to only one user pair [27]. In particular, we let $\chi_{m,i}(t) \in \{0, 1\}$ denote the subchannel assignment indicator. Specifically, $\chi_{m,i}(t) = 1$ if user i is assigned to subchannel m at time slot t and $\chi_{m,i}(t) = 0$, otherwise. A pair of GUEs can share one subchannel simultaneously and each user can receive its data from only one subchannel,

$$\sum_{g=1}^{N} (\chi_{m,2g-1}(t) + \chi_{m,2g}(t)) = 2, \forall m \in \mathcal{M}, \text{ and} \quad \sum_{m=1}^{M} \chi_{m,i}(t) = 1, \forall i \in \mathcal{N}. \tag{1}$$

Then, the superimposed signal sent from the GBS to the pair g $\in \mathcal{G}$ on the subchannel m at time slot t, is given as

$$x_{m,g}(t) = \chi_{m,2g-1}(t)\sqrt{p_{m,2g-1}(t)}s_{m,2g-1}(t) + \chi_{m,2g}(t)\sqrt{p_{m,2g}(t)}s_{m,2g}(t), \tag{2}$$

where $(s_{m,2g-1}(t), s_{m,2g}(t))$ and $(p_{m,2g-1}(t), p_{m,2g}(t))$ are the message signals and powers allocated to the pair g with GUEs $2g-1$ and $2g$ on the subchannel m at time slot t, respectively. The power allocation for each user group must satisfy the following constraints

$$p_{m,2g-1}(t) - p_{m,2g}(t) \geq 0, \quad \forall m, g, t \tag{3}$$

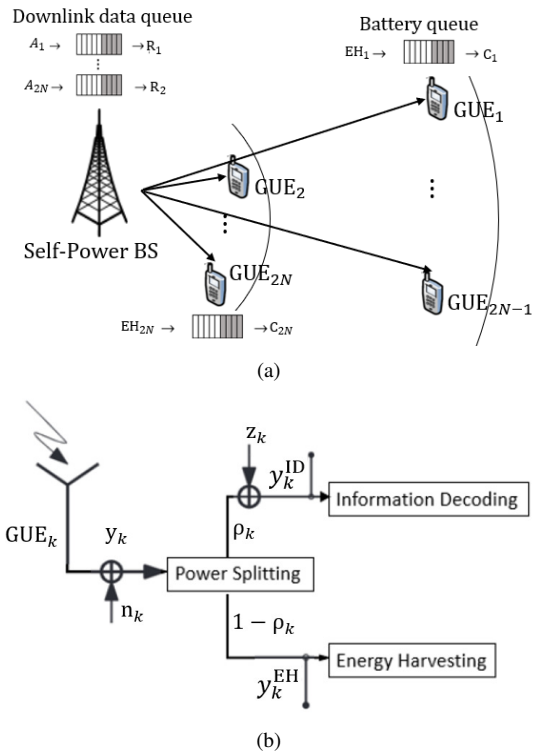

Fig. 1. System model. (a) Cell architecture, (b) Power-splitting SWIPT (PS-SWIPT).

$$P_{0,g}(t) \leq P_g^{max}. \quad \forall g, t \tag{4}$$

Constraint (3) ensures that the transmit power for outer GUE must be greater than that for inner GUE. Constraint (4) indicates the maximum power allocation for each user group, denoted by P_g^{max}. The received signal at GUE k on the subchannel m is given by

$$y_{m,k}(t) = h_{m,k}(t)x_{m,g}(t) + n_{m,k}, \quad \forall k \in \{2g-1, 2g\}, \tag{5}$$

where $h_{m,k}(t)$ denotes the complex channel coefficient from the GBS to GUE k on the subchannel m at time slot t, which is not varying during the time slot but changes from one slot to another. In addition, $n_{m,k}$ represents complex additive white Gaussian noise at GUE k with zero mean and variance σ^2.

In this study, we adopt PS-based SWIPT, in which $1-\rho_k(t)$ and $\rho_k(t)$ are denoted as the PS ratio for the energy harvesting (EH) and for the information decoding (ID) at GUE k at time slot t, respectively. The received signals at GUE k for ID and EH are respectively given by

$$y_{m,k}^{ID}(t) = \sqrt{\rho_k(t)}y_{m,k}(t) + z_{m,k}, \tag{6}$$

$$y_{m,k}^{EH}(t) = \sqrt{1-\rho_k(t)}y_{m,k}(t), \tag{7}$$

where $z_{m,k} \sim \mathcal{CN}\left(0, \varpi^2\right)$ denotes the additional circuit noise introduced by the ID receiver at GUE k, which is also modeled as the additive white Gaussian noise.

The SIC decoding technique is employed to cancel user interference for information decoding at the receiver. The SIC decoding can be determined by the increasing order of channel gains normalized by the noise variance [28]. Thus, the signal-to-interference-plus-noise ratio (SINR) at GUE $2g-1$ (where the signal of GUE $2g$ is treated as noise) is expressed as follows:

$$\text{SINR}_{m,2g-1}(t) = \frac{\chi_{m,2g-1}(t)\rho_{2g-1}(t)p_{m,2g-1}(t)}{\rho_{2g-1}(t)\left[\chi_{m,2g}(t)p_{m,2g}(t) + \mathcal{I}_{m,2g-1}\right] + \mathcal{J}_{m,2g-1}}, \tag{8}$$

where $\mathcal{I}_{m,k} \triangleq \frac{\sigma^2}{|h_{m,k}(t)|^2}$ and $\mathcal{J}_{m,k} \triangleq \frac{\varpi^2}{|h_{m,k}(t)|^2}, \forall k \in \{2g-1, 2g\}$. In addition, at GUE $2g$, the signal of GUE $2g-1$ is decoded with the following SINR:

$$\widetilde{\text{SINR}}_{m,2g-1}(t) = \frac{\chi_{m,2g-1}(t)\rho_{2g}(t)p_{m,2g-1}(t)}{\rho_{2g}(t)\left[\chi_{m,2g}(t)p_{m,2g}(t) + \mathcal{I}_{m,2g}\right] + \mathcal{J}_{m,2g}}. \tag{9}$$

Then, the decoded signal of GUE $2g-1$ is canceled out using the SIC technique; hence, the SINR at GUE $2g$ is expressed as follows:

$$\text{SINR}_{m,2g}(t) = \frac{\chi_{m,2g}(t)\rho_{2g}(t)p_{m,2g}(t)}{\rho_{2g}(t)\mathcal{I}_{m,2g} + \mathcal{J}_{m,2g}}. \tag{10}$$

To ensure a successful SIC, the SINR of GUE $2g$ to decode the signal of GUE $2g-1$ should be no less than that of GUE $2g-1$ to decode its own signal [29], [30]. Thus,

$$\widetilde{\text{SINR}}_{m,2g-1}(t) \geq \text{SINR}_{m,2g-1}(t). \tag{11}$$

Therefore, the achievable rates at GUE $2g-1$ and $2g$ can be written as

$$\begin{aligned} R_{m,2g-1}(t) &= \log_2\left(1 + \text{SINR}_{m,2g-1}(t)\right), \\ R_{m,2g}(t) &= \log_2\left(1 + \text{SINR}_{m,2g}(t)\right). \end{aligned} \tag{12}$$

The linear EH model has commonly been adopted in the literature, where the total harvested energy is linearly proportional to the received RF power. However, the EH circuit presents non-linear end-to-end wireless power transfer in practice [31]. In this study, we consider a practical non-linear EH model [32], which captures the non-linear phenomena caused by the limitations of hardware circuits. Based on this model, the harvested energy of GUE k from subchannel m at time slot t is expressed as follows:

$$\text{EH}_{m,k}(t) = \frac{\frac{H_k^{\max}}{1+e^{-a_k(P_{m,k}^{\text{EH}}(t)-b_k)}} - \frac{H_k^{\max}}{1+e^{a_k b_k}}}{1 - \frac{1}{1+e^{a_k b_k}}}, \tag{13}$$

where $P_{m,k}^{\text{EH}}$ denotes the received power for EH at GUE k, which is given by:

$$P_{m,k}^{\text{EH}}(t) = (1-\rho_k(t))\Big(|h_{m,k}(t)|^2\left(\chi_{m,2g-1}(t)p_{m,2g-1}(t) + \chi_{m,2g}(t)p_{m,2g}(t)\right) + \sigma^2\Big), \tag{14}$$

and $H_k^{\max}$ is the maximum harvested power at GUE k when the EH circuit reaches saturation. In addition, a_k and b_k are parameters related to circuit specifications, such as capacitance, resistance, and the diode turn-on voltage. They can be obtained using a standard curve fitting tool.

C. Queue Model

This paper considers two types of queues: the downlink data queue and the energy queue.

1) Downlink Data Queue at GBS: The GBS separately maintains the data queue for each GUE. In every time slot, the data for each GUE arrives in the queue and is forwarded to the GUE. In particular, the data queue for GUE $i \in \mathcal{N}$ at time slot t, denoted by $Q_i(t)$, evolves as follows:

$$Q_i(t+1) = [Q_i(t) - R_{m,i}(t)]^+ + A_i(t), \tag{15}$$

where $a^+ \triangleq \max\{0, a\}$, $A_i(t)$ is the number of arrived data at time slot t, which is assumed to follow the Poisson distribution with an arrival rate given by $\lambda_i \triangleq \mathbb{E}\{A_i(t)\}$, and $R_{m,i}(t)$ is the service (departure) rate at time slot t.

2) Battery Queue for the GUE: Each GUE consumes battery energy to collect and receive data from the GBS and for EH. The GUE charges its battery energy using PS-SWIPT for every time slot. We assume that the GUEs complete EH at the end of each time slot and consume energy for operation at the beginning of the next time slot. In time slot t, the harvested energy $EH_{m,i}(t)$ cannot be used immediately. We let $B_i(t)$ be the energy stored in the battery of GUE i at the beginning of time slot t. Then, the battery energy $B_i(t+1)$ in time slot $t+1$ can be described as follows:

$$B_i(t+1) = [B_i(t) - C_i(t)]^+ + \mathrm{EH}_{m,i}(t), \tag{16}$$

where $C_i(t)$ denotes the consumed battery energy of the GUE i in time slot t. Moreover, for each GUE i, the consumed battery energy $C_i(t)$ should satisfy the following condition:

$$0 \le C_i(t) \le B_i(t), \forall t \in \{1, 2, \dots\}, \tag{17}$$

which means that the consumed battery energy should be no more than the available battery energy. In addition, battery energy $B_i(t)$ for each GUE satisfies

$$0 \le B_i(t) \le B_i^{max}, \forall t \in \{1, 2, \dots\}, \tag{18}$$

where B_i^{max} represents the maximum battery capacity at GUE i. Under the Constraints (17) and (18), the queue update for $B_i(t)$ in (16) can be rewritten as follows:

$$B_i(t+1) = \min\{B_i(t) - C_i(t) + EH_{m,i}(t), B_i^{max}\}. \tag{19}$$

D. Problem Formulation

This work aims to minimize the long-term time average transmission power at the GBS while supporting the user quality of service, data queue stability, and battery energy availability. To this end, at each time t, we control the subchannel assignment $\boldsymbol{\chi}(t)$, power allocation $\mathbf{P}(t)$, and PS ratio $\boldsymbol{\rho}(t)$. Then, the optimization problem can be stated as follows:

$$\textbf{(P1)} \min_{\boldsymbol{\chi}(t), \mathbf{P}(t), \boldsymbol{\rho}(t)} \quad \lim_{T\to\infty} \frac{1}{T} \sum_{t=0}^{T-1} \sum_{g=1}^{N} \mathbb{E}\{P_{0,g}(t)\} \tag{20}$$

s.t.

$$\lim_{T\to\infty} \frac{1}{T} \sum_{t=0}^{T-1} \mathbb{E}\{R_{m,i}(t)\} \ge R_i^{req}, \quad \forall i \tag{21}$$

$$\lim_{T\to\infty} \frac{1}{T} \sum_{t=0}^{T-1} \mathbb{E}\{B_i(t) - C_i(t) + EH_{m,i}(t)\} \ge \theta_i, \forall i \tag{22}$$

$$p_{m,2g-1}(t) \ge 0, p_{m,2g-1}(t) \ge 0, \quad \forall m, g, t \tag{23}$$

$$0 \le \rho_i(t) \le 1, \quad \chi_{m,i}(t) \in \{0, 1\}, \quad \forall m, i, t \tag{24}$$

$$Q_i(t) \text{ is stable}, \quad \forall i \tag{25}$$

$$(1), (3), (4), (11), \tag{26}$$

where $P_{0,g}(t) \triangleq \chi_{m,2g-1}(t) p_{m,2g-1}(t) + \chi_{m,2g}(t) p_{m,2g}(t)$, $\mathbb{E}\{\cdot\}$ denotes the statistical expectation. In addition, $\boldsymbol{\chi}(t) \triangleq \left[\boldsymbol{\chi}_g(t)\right]_{g\in\mathcal{G}}$ denotes the subchannel assignment matrix, where $\boldsymbol{\chi}_g(t) \triangleq [\chi_{m,2g-1}(t), \chi_{m,2g}(t)]$. Further, $\mathbf{P}(t) \triangleq [\mathbf{p}_g(t)]_{g\in\mathcal{G}}$ represents the power allocation matrix, where $\mathbf{p}_g(t) \triangleq [p_{m,2g-1}(t), p_{m,2g}(t)]$ and $\boldsymbol{\rho}(t) \triangleq [\boldsymbol{\rho}_g(t)]_{g\in\mathcal{G}}$ indicates the PS ratio matrix, where $\boldsymbol{\rho}_g(t) \triangleq [\rho_{2g-1}(t), \rho_{2g}(t)]$. Constraints (21) and (22) require that the minimum long-term average rate for each user i and the expected amount of remaining energy in the battery of each user i should be greater than the required minimum rate R_i^{req} and the minimum energy threshold θ_i, respectively. Constraint (25) indicates that the data queue for each user should be stable. A queue is stable (there is no data overflow) if the long-term average of output data is greater than or equal to the long-term average of the input data [33], which motivates the definition of *mean rate stability*, which is presented in a later section.

Problem **(P1)** is challenging to solve directly. Because it contains continuous variables, $\boldsymbol{P}(t)$ and $\boldsymbol{\rho}(t)$, and discrete variable $\boldsymbol{\chi}(t)$. Therefore, **(P1)** is a mixed-integer programming problem. Second, the expectation operator and non-convex terms appear in the objective function and Constraints (11), (21), and (22). Third, feasible solutions should satisfy the queue stability condition. To address the above challenges, we applied the Lyapunov optimization framework [33], which has advantages compared with other methods, such as stochastic dynamic programming, calculus of variation-based control, and reinforcement learning for stochastic control-type problems. Specifically, the Lyapunov approach can provide a way to solve a long-term stochastic control problem in a way that solves an instantaneous and opportunistic online control problem. In addition, Lyapunov control enables a control that ensures the system stability in terms of various types of real and virtual queues. Furthermore, because of the possibility of online control, Lyapunov control has much less computational complexity.

III. Lyapunov Optimization-based Algorithm

In this section, before applying the Lyapunov optimization to solve Problem **(P1)**, we first transform Constraints (21) and (22) into queue stability problems [33]. In particular, for each user i, the virtual queues for the data rate and battery constraints are denoted by $Y_i(t)$ and $Z_i(t)$, respectively, with the following update equations:

$$Y_i(t+1) = \left[Y_i(t) - R_{m,i}(t) + R_i^{req}\right]^+, \tag{27}$$

$$Z_i(t+1) = \left[Z_i(t) - D_i(t) + \theta_i\right]^+, \tag{28}$$

where $D_i(t) \triangleq B_i(t) - C_i(t) + EH_{m,i}(t)$. According to [33], $Y_i(t)$ and $Z_i(t)$ are mean rate stable if $\lim_{T\to\infty} \frac{\mathbb{E}\{Y_i(T)\}}{T} = 0$ and $\lim_{T\to\infty} \frac{\mathbb{E}\{Z_i(T)\}}{T} = 0$, respectively. Then, using the following lemma, we can prove that Constraints (21) and (22) are satisfied if the corresponding virtual queues are mean rate stable.

Lemma 1. *For all $i \in \mathcal{N}$, if $Y_i(t)$ and $Z_i(t)$ are mean rate stable, Constraints* (21) *and* (22) *are satisfied, respectively.*

Proof. Please see Appendix A. □

To proceed with Lyapunov optimization, we first define a concatenated vector of the general and virtual queues as $\mathbf{\Omega}(t) \triangleq [Q_i(t), B_i(t), Y_i(t), Z_i(t) : i \in \mathcal{N}]$ and then define the corresponding Lyapunov function as follows [33]:

$$L(\mathbf{\Omega}(t)) \triangleq \frac{1}{2}\Bigg[\sum_{i\in\mathcal{N}} w_{1,i}Q_i^2(t) + \sum_{i\in\mathcal{N}} w_{2,i}\left(B_i^{max} - B_i(t)\right)^2 + \sum_{i\in\mathcal{N}} w_{3,i}Y_i^2(t) + \sum_{i\in\mathcal{N}} w_{4,i}Z_i^2(t)\Bigg], \tag{29}$$

where $\{w_{j,i}\}_{j=1}^4$ are positive weights to ensure that the queues are in the same order of magnitude. This function measures queue congestion in the network, which is large when at least one queue backlog is large and is small when all queue backlogs are small. The *one-slot conditional Lyapunov drift* at time slot t can be denoted as

$$\Delta(\mathbf{\Omega}(t)) \triangleq \mathbb{E}\left\{L(\mathbf{\Omega}(t+1)) - L(\mathbf{\Omega}(t))|\mathbf{\Omega}(t)\right\}. \tag{30}$$

This function represents the change in the Lyapunov function from one slot to the next, given the current state $\mathbf{\Omega}(t)$. Then, we define the *drift-plus-penalty* expression, denoted as $\Delta_V(\mathbf{\Omega}(t))$, which is the weighted sum of the conditional Lyapunov drift and total power consumption at time slot t:

$$\Delta_V(\mathbf{\Omega}(t)) \triangleq \Delta(\mathbf{\Omega}(t)) + V\mathbb{E}\left\{\sum_{g=1}^{N} P_{0,g}(t)|\mathbf{\Omega}(t)\right\}, \tag{31}$$

where V is a non-negative control parameter representing how much we emphasize minimizing the transmit power at the GBS. To stabilize the queues while minimizing the transmit power at the GBS, we aim to minimize the drift-plus-penalty function $\Delta_V(\mathbf{\Omega}(t))$. First, we propose an upper bound for the drift.

Lemma 2. *The upper bound of $\Delta_V(\mathbf{\Omega}(t))$ for all t is given by*

$$\begin{aligned}\Delta_V(\mathbf{\Omega}(t)) \le{}& \xi + V\mathbb{E}\left\{\sum_{g=1}^{N} P_{0,g}(t)|\mathbf{\Omega}(t)\right\} \\ &+ \sum_{i\in\mathcal{N}} w_{1,i}Q_i(t)\mathbb{E}\big\{A_i(t) - R_{m,i}(t)|\mathbf{\Omega}(t)\big\} \\ &+ \sum_{i\in\mathcal{N}} w_{2,i}\left(B_i^{max} - B_i(t)\right)\mathbb{E}\left\{C_i(t) - EH_{m,i}(t)|\mathbf{\Omega}(t)\right\} \\ &+ \sum_{i\in\mathcal{N}} w_{3,i}Y_i(t)\mathbb{E}\left\{R_i^{req} - R_{m,i}(t)|\mathbf{\Omega}(t)\right\} \\ &+ \sum_{i\in\mathcal{N}} w_{4,i}Z_i(t)\mathbb{E}\left\{\theta_i - D_i(t)|\mathbf{\Omega}(t)\right\},\end{aligned} \tag{32}$$

where ξ is a positive constant that satisfies the following for all t:

$$\begin{aligned}\xi = \frac{1}{2}\sum_{i\in\mathcal{N}}\Bigg[& w_{1,i}\left(\hat{R}_{m,i}^2 + \hat{A}_i^2\right) + w_{2,i}\left(\hat{C}_i^2 + \widehat{EH}_{m,i}^2\right) \\ &+ w_{3,i}\left((R_{m,i}^{req})^2 + \hat{R}_{m,i}^2\right) + w_{4,i}\left(\hat{B}_i^2 + \widehat{EH}_{m,i}^2 + \frac{\theta_i^2}{2}\right)\Bigg],\end{aligned}$$

with $\hat{A}_i, \hat{C}_i, \widehat{EH}_{m,i}, \hat{R}_{m,i}$, and $\hat{B}_i$ are the maximum values of $\mathbb{E}\{A_i(t)\}, \mathbb{E}\{C_i(t)\}, \mathbb{E}\{EH_{m,i}(t)\}, \mathbb{E}\{R_{m,i}(t)\}$, and $\mathbb{E}\{B_i(t)\}$, respectively.

Proof. Please see Appendix B. □

From the above lemma, the drift-plus-penalty $\Delta_V(\mathbf{\Omega}(t))$ has an upper bound for all t. Thus, instead of minimizing $\Delta_V(\mathbf{\Omega}(t))$ at each time slot, the strategy is to minimize the upper bound given on the right-hand side of (32), which can be accomplished via the concept of the *opportunistic minimization of (conditional) expectation* [33]. Then, the resulting optimization problem at each time slot is stated as follows (the time indicator t is omitted to simplify the notation):

$$\begin{aligned}\textbf{(P2)} \quad \min_{\boldsymbol{\chi},\mathbf{P},\boldsymbol{\rho}} \quad & U(\mathbf{P},\boldsymbol{\rho},\boldsymbol{\chi}) \triangleq \sum_{g=1}^{N} U_g(\boldsymbol{\chi}_g, \boldsymbol{p}_g, \boldsymbol{\rho}_g) \\ \text{s.t.} \quad & (1), (3), (4), (11), (23), (24),\end{aligned}$$

where $U_g(\boldsymbol{\chi}_g, \boldsymbol{p}_g, \boldsymbol{\rho}_g) \triangleq \big(VP_{0,g} - \sum_{k\in\{2g-1,2g\}} \alpha_k R_{m,k} - \sum_{k\in\{2g-1,2g\}} \beta_k \mathrm{EH}_{m,k}\big)$, $\alpha_k \triangleq w_{1,k}Q_k + w_{3,k}Y_k, \beta_k \triangleq w_{2,k}(B_k^{max} - B_k) + w_{4,k}Z_k, \forall k \in \{2g-1, 2g\}$. In this study, we propose a subchannel assignment, power allocation, and PS ratio control to minimize the long-term average power transmit consumption by minimizing the above upper bound. Moreover, the problem only depends on the current queue states, CSI, and battery state information, facilitating an online algorithm design.

It can be observed that Problem **(P2)** is non-convex and highly coupled with three variables: subchannel assignment, power allocation, and PS ratio. In addition, the subchannel assignment variable is binary, which makes the problem even more challenging. To address this difficulty, we decouple the problem into three subproblems: subchannel assignment, power allocation, and PS ratio optimization. First, a low-complexity subchannel assignment algorithm is proposed based on one-to-one matching. Then, for the given subchannel assignment, the power allocation and PS ratio are jointly optimized using AO technique and the solutions can be obtained in closed form or approximated using the low-complexity bisection method. Moreover, the joint optimization of the power allocation and the PS ratio can be performed on each user group, which facilitates an efficient distributed algorithm.

IV. Proposed Online Resource Scheduling Algorithm

A. Matching-based subchannel Assignment

In this subsection, we apply the matching theory to determine the optimal solution for subchannel assignment. For

the given power allocation $\boldsymbol{P}$ and PS ratio $\boldsymbol{\rho}$, optimization Problem **(P2)** with respect to $\boldsymbol{\chi}$ is reformulated as the following maximization problem:

$$\max_{\substack{\chi_{m,i}\in\{0,1\},\\ \forall m,i}} \sum_{g=1}^{N} \big(-VP_{0,g} + \sum_{k\in\{2g-1,2g\}} \alpha_k R_{m,k} + \sum_{k\in\{2g-1,2g\}} \beta_k \mathrm{EH}_{m,k} \big), \tag{33}$$

$$\text{s.t.} \quad (1). \tag{34}$$

In this study, we propose a low-complexity algorithm based on the matching theory [34]. This problem can be formulated as the *one-to-one matching* game between two sets of players, which are the set of user groups $\mathcal{G}$ and set of subchannels $\mathcal{M}$. Formally, the matching model is defined as follows.

Definition 1. *In one-to-one matching, a matching φ is a one-to-one correspondence from the set $\mathcal{G}\cup\mathcal{M}$ onto itself such that the following conditions hold for every $g \in \mathcal{G}$ and $m \in \mathcal{M}$:*

1) $\varphi(g) = m$ if and only if $\varphi(m) = g$;
2) If $\varphi(g) \neq g$, then $\varphi(g) \in \mathcal{M}$;
3) If $\varphi(m) \neq m$, then $\varphi(m) \in \mathcal{G}$.

From the above definition, Condition 1 indicates that user group g is matched with subchannel m if and only if subchannel m is also matched with user group g. Conditions 2 and 3 indicate that any player not matched with itself must be matched with a player in the opposite set.

1) Preference list: In this game, each player first collects information from opposite players, then performs ranking based on preference. The ranked list of preferences is called the *preference list*, which is created according to the objective function presented in (33). Specifically, a user group g prefers subchannel m to m' based on its utility, as follows:

$$m \succ_g m' \Leftrightarrow \Phi_g(m) > \Phi_g(m'), \tag{35}$$

where the utility of the user group g on subchannel m is defined as follows:

$$\Phi_g(m) \triangleq -V \sum_{k\in\{2g-1,2g\}} p_{m,k} + \sum_{k\in\{2g-1,2g\}} \alpha_k R_{m,k} + \sum_{k\in\{2g-1,2g\}} \beta_k \mathrm{EH}_{m,k}, \forall m \in \mathcal{M}, \tag{36}$$

Accordingly, the preference list of user group g on subchannels in $\mathcal{M}$, denoted as $PL^U(g)$, can be generated by sorting the utilities in descending order. The preference list of all user groups in $\mathcal{G}$ on subchannels in $\mathcal{M}$ is denoted as $\boldsymbol{PL}^U = \{PL^U(g)\}_{g\in\mathcal{G}}$. Analogously, the preference for subchannel m on two arbitrary user groups g and $g' \in \mathcal{G}$ is defined as

$$g \succ_m g' \Leftrightarrow \Phi_m(g) > \Phi_m(g'). \tag{37}$$

where the utility of subchannel m on user group g is defined as follows:

$$\Phi_m(g) \triangleq -V \sum_{k\in\{2g-1,2g\}} p_{m,k} + \sum_{k\in\{2g-1,2g\}} \alpha_k R_{m,k} + \sum_{k\in\{2g-1,2g\}} \beta_k \mathrm{EH}_{m,k}, \forall g \in \mathcal{G}. \tag{38}$$

Accordingly, the preference list for subchannel m on the user groups in $\mathcal{G}$ is denoted as $PL^S(m)$. The preference list for all subchannels in $\mathcal{M}$ on user groups in $\mathcal{G}$ is denoted as $\boldsymbol{PL}^S = \{PL^S(m)\}_{m\in\mathcal{M}}$.

Algorithm 1 Matching-based subchannel assignment algorithm

Input: 1. Construct the preference list for user groups $\boldsymbol{PL}^U$ and subchannels $\boldsymbol{PL}^S$.
2. Initialize the set of user groups not matched to any subchannel ($\mathcal{A}^0 \triangleq \mathcal{G}$).

Output: The matching solution.

```
while A^0 ≠ ∅ do
  for g ∈ A^0 do
    User group g proposes to the most preferred subchannel in its preference list PL^U(g), which has never before rejected it;
  end for
  for m ∈ M do
    if subchannel m has not been matched with any user group then
      Subchannel m keeps the proposed user group g and removes it from A^0;
    else if subchannel m has been currently matched with a group g̃
      if subchannel m prefers g to g̃ according to its preference list PL^S(m) then
        Subchannel m keeps g and rejects g̃;
        Remove g from A^0 and keep g̃ in A^0;
        Update PL^U(g̃) by removing m;
      else
        Subchannel m keeps g̃ continually and rejects g;
        Update PL^U(g) by removing m;
      end if
    end if
  end for
end while
```

2) Matching-based Subchannel Assignment Algorithm: After the preference list for each user group and subchannel is constructed, the matching algorithm based on the well-known Gale-Shapley algorithm [34], [35] is adopted. Specifically, $\mathcal{A}^0$ denotes as the set of user groups not matched to any subchannel. Each unmatched user group sends a proposal to the most preferred subchannel according to its preference list during the matching process. When any subchannel has not been matched with any user group, the new proposal user group is kept as a partner. Otherwise, when it has been currently matched with a group, it chooses the most preferred group based on its preference list and rejects the other group. The process continues until no user group is left in $\mathcal{A}^0$ (every user group has a partner). The algorithm for subchannel assignment is summarized in Algorithm 1. The proposed matching algorithm focuses on the one-to-one matching between user groups and subchannels, whereas other studies have focused on many-to-many (one) matching with *peer effects*, where the agents care more about their own

matching [36], [37]. The traditional stability (demonstrated in Definition 3, Subsection IV-D) cannot be guaranteed in such a matching type.

B. Optimizing Power Allocation in Each User Group

For the given PS ratio $\boldsymbol{\rho}$ and subchannel assignment $\boldsymbol{\chi}$, the power allocation can be performed over each user group. Specifically, the minimization Problem **(P2)** in a user group $g \in \mathcal{G}$ with respect to $(p_{m,2g-1}, p_{m,2g})$ can be equivalently rewritten as the following maximization problem:

$$\begin{aligned}\min_{p_{m,2g-1},p_{m,2g}} \quad & V(p_{m,2g-1}+p_{m,2g}) \\ & - \alpha_{2g-1}\log_2\left(1+\frac{\rho_{2g-1}p_{m,2g-1}}{\rho_{2g-1}\left(p_{2g}+\mathcal{I}_{m,2g-1}\right)+\mathcal{J}_{m,2g-1}}\right) \\ & - \alpha_{2g}\log_2\left(1+\frac{\rho_{2g}p_{m,2g}}{\rho_{2g}\mathcal{I}_{m,2g}+\mathcal{J}_{m,2g}}\right) \\ & - \frac{\beta_{2g-1}B_{2g-1}H_{2g-1}^{max}}{1+e^{-a_{2g-1}\left(P_{m,2g-1}^{EH}-b_{2g-1}\right)}} - \frac{\beta_{2g}B_{2g}H_{2g}^{max}}{1+e^{-a_{2g}\left(P_{m,2g}^{EH}-b_{2g}\right)}} \end{aligned} \tag{39}$$

$$\text{s.t.} \quad p_{m,2g-1}+p_{m,2g} \le P_g^{max}, \tag{40}$$

$$p_{m,2g-1}-p_{m,2g} \ge 0, \tag{41}$$

$$p_{m,2g-1} \ge 0, p_{m,2g} \ge 0, \tag{42}$$

where $P_{m,k}^{\text{EH}} = (1-\rho_k)\left(|h_{m,k}|^2\left(p_{m,2g-1}+p_{m,2g}\right)+\sigma^2\right), \forall k \in \{2g-1, 2g\}$. Because this problem is non-convex, it is difficult to solve analytically. To address this challenge, the AO algorithm is adopted to determine the optimal $(p_{m,2g-1}, p_{m,2g})$. However, we first define a new variable p_g^{sum} such that $p_{m,2g-1} = p_g^{sum} - p_{m,2g}$. With such a new variable, we can obtain solutions more efficiently by optimizing $(p_{m,2g}, p_g^{sum})$ instead of $(p_{m,2g}, p_{m,2g-1})$. The solutions can be found in an alternative manner as follows.

1) Optimizing $p_{m,2g}$ for a Given p_g^{sum}: For a given p_g^{sum}, the optimization problem w.r.t. $p_{m,2g}$ is written as follows:

$$\begin{aligned}\min_{p_{m,2g}} \quad & f(p_{m,2g}) \triangleq \alpha_{2g-1}\log_2\left(\rho_{2g-1}p_{m,2g}+\nu_{m,2g-1}\right) \\ & \qquad - \alpha_{2g}\log_2\left(\rho_{2g}p_{m,2g}+\nu_{m,2g}\right) \end{aligned} \tag{43}$$

$$\text{s.t.} \quad 0 \le p_{m,2g} \le p_g^{sum}/2, \tag{44}$$

where $\nu_{m,2g-1} \triangleq \rho_{2g-1}\mathcal{I}_{m,2g-1}+\mathcal{J}_{m,2g-1}, \nu_{m,2g} \triangleq \rho_{2g}\mathcal{I}_{m,2g}+\mathcal{J}_{m,2g}$. To solve this problem, we first compute the first-order derivative of $f(p_{m,2g})$ with respect to (w.r.t.) $p_{m,2g}$ and obtain

$$\begin{aligned} & f'(p_{m,2g}) \\ & = \frac{\left[\begin{array}{r}\left(\alpha_{2g-1}-\alpha_{2g}\right)\rho_{2g-1}\rho_{2g}p_{m,2g}+\alpha_{2g-1}\rho_{2g-1}\nu_{m,2g} \\ -\alpha_{2g}\rho_{2g}\nu_{m,2g-1}\end{array}\right]}{\log(2)\left(\rho_{2g-1}p_{m,2g}+\nu_{m,2g-1}\right)\left(\rho_{2g}p_{m,2g}+\nu_{m,2g}\right)}. \end{aligned} \tag{45}$$

We define the numerator of (45) as

$$\begin{aligned} F(p_{m,2g}) \triangleq & \left(\alpha_{2g-1}-\alpha_{2g}\right)\rho_{2g-1}\rho_{2g}p_{m,2g} \\ & + \alpha_{2g-1}\rho_{2g-1}\nu_{m,2g} - \alpha_{2g}\rho_{2g}\nu_{m,2g-1}. \end{aligned} \tag{46}$$

We propose the following lemma to obtain the optimal $p_{m,2g}$.

Lemma 3. *On the feasible region $\left[0, p_g^{sum}/2\right]$, the function F is a strictly increasing function if $(\alpha_{2g-1}-\alpha_{2g})\rho_{2g-1}\rho_{2g} > 0$ and is a constant function if $(\alpha_{2g-1}-\alpha_{2g})\rho_{2g-1}\rho_{2g} = 0$. Otherwise, it is a strictly decreasing function.*

Proof. Please see Appendix C. □

From the above lemma, according to the monotonicity of the function $F(p_{m,2g})$, we proceed to determine the optimal solution $p_{m,2g}^*$ as follows:

Case 1: $\alpha_{2g-1} > \alpha_{2g}$ and $\rho_{2g-1}\rho_{2g} \neq 0$, i.e., $F(p_{m,2g})$ is strictly increasing on $\left[0, p_g^{sum}/2\right]$:

- If $F(0) > 0$, then $F(p_{m,2g}) > 0, \forall p_{m,2g} \in \left[0, p_g^{sum}/2\right]$. As a result, $f'(p_{m,2g}) > 0, \forall p_{m,2g} \in \left[0, p_g^{sum}/2\right]$, i.e., f is strictly increasing. Therefore, $p_{m,2g}^* = 0$.
- If $F(0) \le 0 \le F(p_g^{sum}/2)$, then $p_{m,2g}^*$ is the solution to the equation $F(p_{m,2g}) = 0$. Solving this equation yields $p_{m,2g}^* = \frac{\alpha_{2g}\rho_{2g}\nu_{m,2g-1}-\alpha_{2g-1}\rho_{2g-1}\nu_{m,2g}}{(\alpha_{2g-1}-\alpha_{2g})\rho_{2g-1}\rho_{2g}}$.
- If $F(p_g^{sum}/2) < 0$, then $F(p_{m,2g}) < 0, \forall p_{m,2g} \in \left[0, p_g^{sum}/2\right]$. As a result, $f'(p_{m,2g}) < 0, \forall p_{m,2g} \in \left[0, p_g^{sum}/2\right]$. Therefore, $p_{m,2g}^* = p_g^{sum}/2$.

Case 2: $\alpha_{2g-1} < \alpha_{2g}$ and $\rho_{2g-1}\rho_{2g} \neq 0$, i.e., $F(p_{m,2g})$ is strictly decreasing on $\left[0, p_g^{sum}/2\right]$:

- If $F(p_g^{sum}/2) > 0$, then $F(p_{m,2g}) > 0, \forall p_{m,2g} \in \left[0, p_g^{sum}/2\right]$. As a result, $f'(p_{m,2g}) > 0, \forall p_{m,2g} \in \left[0, p_g^{sum}/2\right]$. Thus, $p_{m,2g}^* = 0$.
- If $F(p_g^{sum}/2) \le 0 \le F(0)$, then $p_{m,2g}^* = \arg\min\{f(0), f(p_g^{sum}/2)\}$.
- If $F(0) < 0$, then $F(p_{m,2g}) < 0, \forall p_{m,2g} \in \left[0, p_g^{sum}/2\right]$. As a result, $f'(p_{m,2g}) < 0, \forall p_{m,2g} \in \left[0, p_g^{sum}/2\right]$. Thus, $p_{m,2g}^* = p_g^{sum}/2$.

Case 3: $\alpha_{2g-1} = \alpha_{2g}$ or $\rho_{2g-1}\rho_{2g} = 0$:

- If $\alpha_{2g-1}\rho_{2g-1}\nu_{m,2g} - \alpha_{2g}\rho_{2g}\nu_{m,2g-1} \ge 0$, then $f'(p_{m,2g}) \ge 0$, i.e., f is increasing on $\left[0, p_g^{sum}/2\right]$. Thus, $p_{m,2g}^* = 0$.
- If $\alpha_{2g-1}\rho_{2g-1}\nu_{m,2g} - \alpha_{2g}\rho_{2g}\nu_{m,2g-1} < 0$, then $f'(p_{m,2g}) < 0$, i.e., f is strictly decreasing on $\left[0, p_g^{sum}/2\right]$. Thus, $p_{m,2g}^* = p_g^{sum}/2$.

2) Optimizing p_g^{sum} for a Given $p_{m,2g}$: This part investigates the optimal p_g^{sum}. Given the optimal $p_{m,2g}$ found in the previous part, we can derive the optimal p_g^{sum} by solving the following problem:

$$\begin{aligned}\min_{p_g^{sum}} \quad & f_s(p_g^{sum}) \triangleq \\ & Vp_g^{sum} - \alpha_{2g-1}\log_2\left(\rho_{2g-1}p_g^{sum}+\nu_{m,2g-1}\right) \\ & - \frac{\beta_{2g-1}B_{2g-1}H_{2g-1}^{max}}{1+e^{-\eta_{m,2g-1}p_g^{sum}-\xi_{2g-1}}} - \frac{\beta_{2g}B_{2g}H_{2g}^{max}}{1+e^{-\eta_{m,2g}p_g^{sum}-\xi_{2g}}} \end{aligned} \tag{47}$$

$$\text{s.t.} \quad 2p_{m,2g} \le p_g^{sum} \le P_g^{max}, \tag{48}$$

where $\eta_{m,k} \triangleq a_k(1-\rho_k)|h_{m,k}|^2$, $\xi_k \triangleq a_k\left[(1-\rho_k)\sigma^2 - b_k\right]$. Computing the first-order derivative of $f_s(p_g^{sum})$ w.r.t. p_g^{sum} yields

$$f_s'(p_g^{sum}) = V - \frac{\alpha_{2g-1}\rho_{2g-1}}{\log(2)\left(\rho_{2g-1}p_g^{sum}+\nu_{m,2g-1}\right)}$$

$$- \frac{\eta_{m,2g-1}\beta_{2g-1}B_{2g-1}H_{2g-1}^{max}e^{-\eta_{m,2g-1}p_g^{sum}-\xi_{2g-1}}}{\left(1+e^{-\eta_{m,2g-1}p_g^{sum}-\xi_{2g-1}}\right)^2} - \frac{\eta_{m,2g}\beta_{2g}B_{2g}H_{2g}^{max}e^{-\eta_{m,2g}p_g^{sum}-\xi_{2g}}}{\left(1+e^{-\eta_{m,2g}p_g^{sum}-\xi_{2g}}\right)^2}. \quad (49)$$

Lemma 4. *The function $f_s(p_g^{sum})$ is convex.*

Proof. Please see Appendix D. □

From the above lemma, as f_s is convex on $[2p_{m,2g}, p_g^{sum}]$, f_s' is increasing on this feasible region. Some specific cases can occur, as follows.

- If $f_s'(2p_{m,2g}) \le 0 \le f_s'(P_g^{max})$, the optimal p_g^{sum} can be found by solving the equation $f_s'(p_g^{sum}) = 0$. This equation can be solved using the bisection method.
- If $f_s'(2p_{m,2g}) > 0$, as f_{2g-1}' is increasing, $f_s'(p_g^{sum}) \ge f_s'(0) > 0, \forall p_g^{sum} \in [2p_{m,2g}, p_g^{sum}]$, implying that f_s is strictly increasing on $[2p_{m,2g}, p_g^{sum}]$, then $p_g^{sum} = 2p_{m,2g}$ is optimal.
- If $f_s'(P_g^{max}) < 0$, f_s is strictly decreasing on $[2p_{m,2g}, p_g^{sum}]$, then $p_g^{sum} = P_g^{max}$ is optimal.

C. Optimizing the Power Split Ratio in Each User Group

For a given power allocation $\boldsymbol{P}$ and subchannel assignment $\boldsymbol{\chi}$, Problem **(P2)** can be equivalently reduced to the following maximization problem:

$$\min_{\substack{\rho_{2g-1},\\ \rho_{2g}}} - \alpha_{2g-1}\log_2\left(1+\frac{\rho_{2g-1}p_{m,2g-1}}{\left[\rho_{2g-1}\left(p_{m,2g}+\mathcal{I}_{m,2g-1}\right)+\mathcal{J}_{m,2g-1}\right]}\right) - \alpha_{2g}\log_2\left(1+\frac{\rho_{2g}p_{m,2g}}{\rho_{2g}\mathcal{I}_{m,2g}+\mathcal{J}_{m,2g}}\right) - \frac{\beta_{2g-1}B_{2g-1}H_{2g-1}^{max}}{1+e^{-a_{2g-1}\left(P_{m,2g-1}^{EH}-b_{2g-1}\right)}} - \frac{\beta_{2g}B_{2g}H_{2g}^{max}}{1+e^{-a_{2g}\left(P_{m,2g}^{EH}-b_{2g}\right)}} \quad (50)$$

$$\text{s.t.} \quad \rho_{2g-1}\rho_{2g}\mathcal{I}_{m,2g-1} + \rho_{2g}\mathcal{J}_{m,2g-1} \ge \rho_{2g-1}\rho_{2g}\mathcal{I}_{m,2g} + \rho_{2g-1}\mathcal{J}_{m,2g}, \quad (51)$$

$$0 \le \rho_{2g-1} \le 1, 0 \le \rho_{2g} \le 1, \quad (52)$$

where $P_{m,k}^{\text{EH}} = (1-\rho_k)\left(|h_{m,k}|^2\left(p_{m,2g-1}+p_{m,2g}\right)+\sigma^2\right), \forall k \in \{2g-1, 2g\}$. Constraint (51) is rewritten from Constraint (11) of **(P1)**.

1) Optimizing ρ_{2g-1} for given ρ_{2g}: Given a fixed ρ_{2g}, the optimization problem w.r.t. ρ_{2g-1} is written as follows:

$$\min_{\rho_{2g-1}} \quad f_{\rho_{2g-1}}(\rho_{2g-1}) \triangleq - \alpha_{2g-1}\log_2\left(1+\frac{\rho_{2g-1}p_{m,2g-1}}{\rho_{2g-1}\left(p_{m,2g}+\mathcal{I}_{m,2g-1}\right)+\mathcal{J}_{m,2g-1}}\right) - \frac{\beta_{2g-1}B_{2g-1}H_{2g-1}^{max}}{1+e^{-a_{2g-1}\left(P_{m,2g-1}^{EH}-b_{2g-1}\right)}} \quad (53)$$

$$\text{s.t.} \quad \rho_{2g-1} \in \mathcal{R}_{2g-1}. \quad (54)$$

The feasible region $\mathcal{R}_{2g-1}$ can be determined as follows. From (51), we have

$$\rho_{2g-1}\left(\rho_{2g}\mathcal{I}_{m,2g}+\mathcal{J}_{m,2g}-\rho_{2g}\mathcal{I}_{m,2g-1}\right) \le \rho_{2g}\mathcal{J}_{m,2g-1}. \quad (55)$$

If $\rho_{2g}\mathcal{I}_{m,2g}+\mathcal{J}_{m,2g}-\rho_{2g}\mathcal{I}_{m,2g-1} > 0$, the upper bound of ρ_{2g-1} can be derived from (55) as

$$\rho_{2g-1} \le \frac{\rho_{2g}\mathcal{J}_{m,2g-1}}{\rho_{2g}\mathcal{I}_{m,2g}+\mathcal{J}_{m,2g}-\rho_{2g}\mathcal{I}_{m,2g-1}}. \quad (56)$$

Combined with (52), the feasible region for ρ_{2g-1} is $\mathcal{R}_{2g-1} = \left[0, \rho_{2g-1}^{max}\right]$ where $\rho_{2g-1}^{max} \triangleq \min\left\{\frac{\rho_{2g}\mathcal{J}_{m,2g-1}}{\rho_{2g}\mathcal{I}_{m,2g}+\mathcal{J}_{m,2g}-\rho_{2g}\mathcal{I}_{m,2g-1}}, 1\right\}$. For the case $\rho_{2g}\mathcal{I}_{m,2g}+\mathcal{J}_{m,2g}-\rho_{2g}\mathcal{I}_{m,2g-1} \le 0$, the inequality in (55) implies that $\rho_{2g}\mathcal{J}_{m,2g-1} \ge 0$, which holds for all $\rho_{2g-1} \in [0,1]$. Thus, the feasible region is $\mathcal{R}_{2g-1} = [0,1]$. After determining the feasible region for ρ_{2g-1}, we can derive the optimal solution. First, computing the first-order derivative of $f_{\rho_2 g-1}$ w.r.t. ρ_{2g-1} yields

$$f_{\rho_{2g-1}}'(\rho_{2g-1}) = \frac{-\alpha_{2g-1}}{\log(2)}\left[\frac{\mathcal{E}_{2g-1}}{\rho_{2g-1}\mathcal{E}_{2g-1}+\mathcal{J}_{m,2g-1}} - \frac{\mathcal{F}_{2g-1}}{\rho_{2g-1}\mathcal{F}_{2g-1}+\mathcal{J}_{m,2g-1}}\right] + \frac{\beta_{2g-1}B_{2g-1}H_{2g-1}^{max}a_{2g-1}\mathcal{G}_{2g-1}e^{-a_{2g-1}[(1-\rho_{2g-1})\mathcal{G}_{2g-1}-b_{2g-1}]}}{\left(1+e^{-a_{2g-1}[(1-\rho_{2g-1})\mathcal{G}_{2g-1}-b_{2g-1}]}\right)^2}, \quad (57)$$

where $\mathcal{E}_{2g-1} \triangleq p_{m,2g-1}+p_{m,2g}+\mathcal{I}_{m,2g-1}$, $\mathcal{F}_{2g-1} \triangleq p_{m,2g}+\mathcal{I}_{m,2g-1}$, and $\mathcal{G}_{2g-1} \triangleq |h_{m,2g-1}|^2\left(p_{m,2g-1}+p_{m,2g}\right)+\sigma^2$. The following lemma demonstrates the convexity of the function $f_{\rho_{2g-1}}$.

Lemma 5. *The function $f_{\rho_{2g-1}}(\rho_{2g-1})$ is convex.*

Proof. The proof is similar to Lemma 4. □

Using the above lemma, we provide the solution for both feasible regions as follows:

- *Feasible region 1:* $\mathcal{R}_{2g-1} = \left[0, \rho_{2g-1}^{max}\right]$
  As $f_{\rho_{2g-1}}$ is convex on $\mathcal{R}_{2g-1}$, $f_{\rho_{2g-1}}'$ is increasing on $\mathcal{R}_{2g-1}$. Some specific cases can occur, as follows.
  - If $f_{\rho_{2g-1}}'(0) \le 0 \le f_{\rho_{2g-1}}'(\rho_{2g-1}^{max})$, the optimal ρ_{2g-1}^* can be found by solving equation $f_{\rho_{2g-1}}'(\rho_{2g-1}) = 0$. This equation can be solved using the bisection method.
  - If $f_{\rho_{2g-1}}'(0) > 0$, we have $f_{\rho_{2g-1}}'(\rho_{2g-1}) \ge f_{\rho_{2g-1}}'(0) > 0, \forall \rho_{2g-1} \in \mathcal{R}_{2g-1}$ (as f_{2g-1}' is increasing). Thus, $f_{\rho_{2g-1}}$ is strictly increasing, and $\rho_{2g-1}^* = 0$ is optimal.
  - If $f_{\rho_{2g-1}}'(\rho_{2g-1}^{max}) < 0$ and $f_{\rho_{2g-1}}$ is strictly decreasing, then $\rho_{2g-1}^* = \rho_{2g-1}^{max}$ is optimal.
- *Feasible region 2:* $\mathcal{R}_{2g-1} = [0,1]$
  The solution for the second region $\mathcal{R}_{2g-1} = [0,1]$ can be obtained similarly.
  - If $f_{\rho_{2g-1}}'(0) \le 0 \le f_{\rho_{2g-1}}'(1)$, the optimal ρ_{2g-1}^* can be found by solving equation $f_{\rho_{2g-1}}'(\rho_{2g-1}) = 0$ using the bisection method.
  - If $f_{\rho_{2g-1}}'(0) > 0$, we have $f_{\rho_{2g-1}}'(\rho_{2g-1}) \ge f_{\rho_{2g-1}}'(0) > 0, \forall \rho_{2g-1} \in \mathcal{R}_{2g-1}$ (as f_{2g-1}' is increasing). Thus, $f_{\rho_{2g-1}}$ is strictly increasing, and $\rho_{2g-1}^* = 0$ is optimal.

– If $f'_{\rho_{2g-1}}(1) < 0$ and $f_{\rho_{2g-1}}$ is strictly decreasing, then $\rho^*_{2g-1} = 1$ is optimal.

2) Optimizing ρ_{2g} for a Given ρ_{2g-1}: Finding the optimal value of ρ_{2g} is also performed similarly. Given a fixed ρ_{2g-1}, the optimization problem w.r.t. ρ_{2g} is written as follows:

$$\min_{\rho_{2g}} \quad f_{\rho_{2g}}(\rho_{2g}) \triangleq$$
$$-\alpha_{2g}\log_2\left(1+\frac{\rho_{2g}p_{m,2g}}{\rho_{2g}\mathcal{I}_{m,2g}+\mathcal{J}_{m,2g}}\right)-\frac{\beta_{2g}B_{2g}H_{2g}^{max}}{1+e^{-a_{2g}\left(P^{EH}_{m,2g}-b_{2g}\right)}} \tag{58}$$

$$\text{s.t.} \quad \rho_{2g} \in \mathcal{R}_{2g}. \tag{59}$$

The feasible region $\mathcal{R}_{2g}$ can be determined as follows. From (51), we have

$$\rho_{2g}\left(\rho_{2g-1}\mathcal{I}_{m,2g-1}+\mathcal{J}_{m,2g-1}-\rho_{2g-1}\mathcal{I}_{m,2g}\right) \geq \rho_{2g-1}\mathcal{J}_{m,2g}. \tag{60}$$

If $\rho_{2g-1}\mathcal{I}_{m,2g-1}+\mathcal{J}_{m,2g-1}-\rho_{2g-1}\mathcal{I}_{m,2g} > 0$, the lower bound of ρ_{2g} can be derived from (60) as

$$\rho_{2g} \geq \frac{\rho_{2g-1}\mathcal{J}_{m,2g}}{\rho_{2g-1}\mathcal{I}_{m,2g-1}+\mathcal{J}_{m,2g-1}-\rho_{2g-1}\mathcal{I}_{m,2g}}. \tag{61}$$

Combined with (52), the feasible region for ρ_{2g} is $\mathcal{R}_{2g} = \left[\rho_{2g}^{min}, 1\right]$ where

$$\rho_{2g}^{min} \triangleq \frac{\rho_{2g-1}\mathcal{J}_{m,2g}}{\rho_{2g-1}\mathcal{I}_{m,2g-1}+\mathcal{J}_{m,2g-1}-\rho_{2g-1}\mathcal{I}_{m,2g}}. \tag{62}$$

For $\rho_{2g-1}\mathcal{I}_{m,2g-1}+\mathcal{J}_{m,2g-1}-\rho_{2g-1}\mathcal{I}_{m,2g} \leq 0$, this case cannot occur because we always have $\rho_{2g-1}\mathcal{I}_{m,2g-1}+\mathcal{J}_{m,2g-1}-\rho_{2g-1}\mathcal{I}_{m,2g} = \rho_{2g-1}\frac{\sigma^2}{|h_{m,2g-1}|^2}+\frac{\varpi^2}{|h_{m,2g-1}|^2}-\rho_{2g-1}\frac{\sigma^2}{|h_{m,2g}|^2} > 0$, as $|h_{m,2g-1}|^2 < |h_{m,2g}|^2$. Thus, we can conclude that the feasible region for ρ_{2g} is $\mathcal{R}_{2g} = [\rho_{2g}^{min}, 1]$. Next, taking the first-order derivative of $f_{\rho_{2g}}(\rho_{2g})$ w.r.t. ρ_{2g} yields

$$f'_{\rho_{2g}}(\rho_{2g}) = \frac{-\alpha_{2g}}{\log(2)}\left[\frac{\mathcal{E}_{2g}}{\rho_{2g}\mathcal{E}_{2g}+\mathcal{J}_{m,2g}}-\frac{\mathcal{I}_{m,2g}}{\rho_{2g}\mathcal{I}_{m,2g}+\mathcal{J}_{m,2g}}\right] + \frac{\beta_{2g}B_{2g}H_{2g}^{max}a_{2g}\mathcal{G}_{2g}e^{-a_{2g}[(1-\rho_{2g})\mathcal{G}_{2g}-b_{2g}]}}{\left(1+e^{-a_{2g}[(1-\rho_{2g})\mathcal{G}_{2g}-b_{2g}]}\right)^2}, \tag{63}$$

where $\mathcal{E}_{2g} \triangleq p_{m,2g}+\mathcal{I}_{m,2g}$ and $\mathcal{G}_{2g} \triangleq |h_{m,2g}|^2\left(p_{m,2g-1}+p_{m,2g}\right)+\sigma^2$. Similarly, we can prove that the function $f_{\rho_{2g}}(\rho_{2g})$ is convex. The proof is omitted here for brevity. Using the convexity of the function $f_{\rho_{2g}}(\rho_{2g})$, we provide the solution for the feasible region $\mathcal{R}_{2g} = [\rho_{2g}^{min}, 1]$. As $f_{\rho_{2g}}$ is convex on $\mathcal{R}_{2g}$, $f'_{\rho_{2g}}$ is increasing on $\mathcal{R}_{2g}$. Some specific cases can occur, as follows.

- If $f'_{\rho_{2g}}(\rho_{2g}^{min}) \leq 0 \leq f'_{\rho_{2g}}(1)$, the optimal ρ^*_{2g} can be found by solving the equation $f'_{\rho_{2g}}(\rho_{2g}) = 0$. This equation can be solved using the bisection method.
- If $f'_{\rho_{2g}}(\rho_{2g}^{min}) > 0$, we have $f'_{\rho_{2g}}(\rho_{2g}) \geq f'_{\rho_{2g}}(\rho_{2g}^{min}) > 0, \forall \rho_{2g} \in \mathcal{R}_{2g}$ (as f'_{2g-1} is increasing). Thus, $f_{\rho_{2g}}$ is strictly increasing, then $\rho^*_{2g} = \rho_{2g}^{min}$ is optimal.
- If $f'_{\rho_{2g}}(1) < 0$ and $f_{\rho_{2g}}$ is strictly decreasing, then $\rho^*_{2g} = 1$ is optimal.

Finally, we discuss the distributed implementation of Algorithm 2. As shown in Algorithm 2, except for the update of subchannel assignment, the AO-based algorithm in Step 2 can be implemented parallelly and distributedly for each user group. The proposed energy-efficient control with SWIPT-NOMA is summarized in Algorithm 2, and its flow chart is illustrated in Fig. 2.

Algorithm 2 Proposed energy-efficient control with SWIPT-NOMA

Input: 1. The initial matching states for user groups are set unmatched.
2. Initialize a feasible point $(\boldsymbol{P}^0, \boldsymbol{\rho}^0)$, set the iteration index $\tau = 0$; tolerance $\varepsilon > 0$.
3. Compute the objective value in **(P2)**, i.e., $U(\mathbf{P}^0, \boldsymbol{\rho}^0, \boldsymbol{\chi}^0)$

Output: The solution $(\boldsymbol{\chi}^*, \boldsymbol{P}^*, \boldsymbol{\rho}^*)$.

1: **Step 1:** *Subchannel assignment*
2: For given $(\boldsymbol{P}, \boldsymbol{\rho})$, obtain the matching state $\boldsymbol{\chi}$ using **Algorithm 1**.
3: **Step 2:** *Joint power allocation and PS ratio*
4: **Repeat**
5: **for** $g \in \mathcal{G}$
6: For a given $\left(\rho^\tau_{2g-1}, \rho^\tau_{2g}\right)$ and current matching state, update $\left(p^{\tau+1}_{m,2g-1}, p^{\tau+1}_{m,2g}\right)$ with solutions given in **Subsection IV-B**;
7: For a given $\left(p^{\tau+1}_{m,2g-1}, p^{\tau+1}_{m,2g}\right)$ and current matching state, update $\left(\rho^{\tau+1}_{2g-1}, \rho^{\tau+1}_{2g}\right)$ with solutions in **Subsection IV-C**;
8: **end for**
9: Update $U(\mathbf{P}^{\tau+1}, \boldsymbol{\rho}^{\tau+1}, \boldsymbol{\chi}^{\tau+1})$
10: $\tau \leftarrow \tau + 1$;
11: **Until** $|U(\mathbf{P}^{\tau+1}, \boldsymbol{\rho}^{\tau+1}, \boldsymbol{\chi}^{\tau+1}) - U(\mathbf{P}^{\tau}, \boldsymbol{\rho}^{\tau}, \boldsymbol{\chi}^{\tau})| < \varepsilon$.

D. Theoretical Analysis

1) Convergence analysis: To analyze the stability of the proposed matching algorithm (Algorithm 1), we first define *stable* matching [35] and prove that Algorithm 1 converges to stable matching.

Definition 2 ([35], p. 21)**.** *Given a matching φ, a user group g and subchannel block the matching φ if they prefer to be matched with each other, but are not matched under φ (i.e., $m \succ_g \varphi(g)$ and $g \succ_m \varphi(m)$). The pair (g, m) is called a blocking pair.*

Definition 3 ([35], p. 21)**.** *A matching φ is stable if no blocking pair exists.*

The following theorem states that the final matching φ obtained from Algorithm 1 is stable.

Theorem 1 (Convergence)**.** *Algorithm 1 converges to a stable matching φ within a finite number of iterations.*

Proof. First, we can observe that Algorithm 1 eventually converges to matching after a finite number of iterations because the number of user groups and subchannels is finite, and no user group proposes more than once to any subchannel. In addition, the outcome is matching because at each step, each user group is matched with at most one subchannel, and each

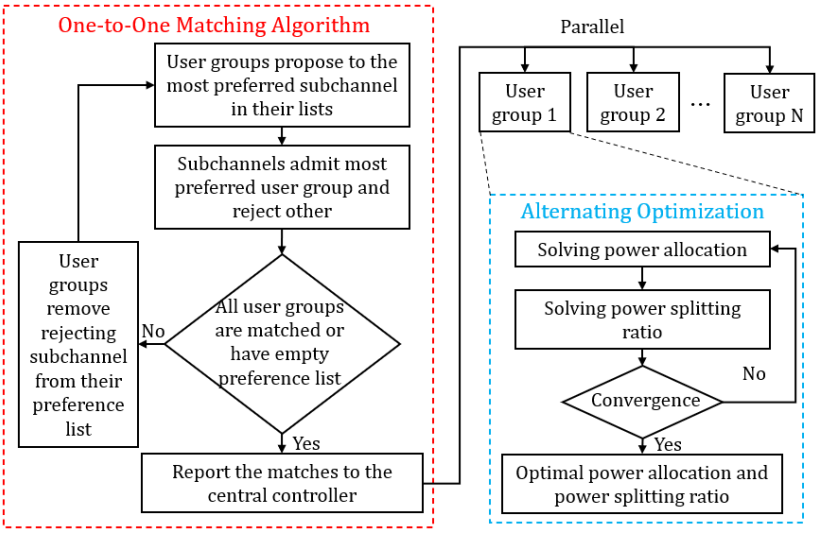

Fig. 2. Flow chart of Algorithm 2.

subchannel is matched with at most one user group. Second, we prove that the final matching φ generated by the algorithm is stable. Suppose that a user group g and subchannel m are not matched under φ, but g prefers to be matched with m instead of the currently assigned partner under φ. This case implies that m is acceptable to g. Then, g proposes to m before proposing to the current partner. As g was not matched with m when the algorithm ended, this implies that g was rejected by m. Therefore, m must have been matched with $\tilde{g}$, providing better utility than that offered by g. Therefore, m and g do not block the matching φ. In other words, the matching φ is stable, which completes the proof. □

Next, we discuss the optimality of the matching algorithm, which can be observed using the concept of *weak Pareto optimality* [38]. The optimality properties of the stable matching hold for the proposing side (i.e., user groups). For every g, we let $u_g(\varphi) \triangleq \Phi_g(\varphi(g))$ denote the utility of user group g achieved by the matching φ and $\boldsymbol{u} \triangleq [u_1, \ldots, u_g, \ldots, u_N]^T$. The definition of weak Pareto optimality is presented as follows.

Definition 4 ([39]). *A matching φ is weak Pareto optimal if no other matching φ' exists with $\boldsymbol{u}(\varphi') \geq \boldsymbol{u}(\varphi)$, where the inequality is component-wise and strict for at least one user.*

Theorem 2 (Weak Pareto optimal)**.** *The stable matching φ obtained from Algorithm 1 is weak Pareto optimal.*

Proof. We assume a matching φ' exists, providing better utility than φ. Then, there is a user group g matched with a subchannel m under φ, i.e., $\varphi(g) = m$, and another subchannel m' is matched with g under φ' (i.e., $\varphi'(g) = m'$). By this assumption, we have $u_g(\varphi') > u_g(\varphi)$, which is equivalent to $\Phi_g(m') > \Phi_g(m)$ (i.e., $m' \succ_g m$). Under the matching φ, we suppose that m' is matched with some user group $\tilde{g}$. Because m is matched with g under φ', $\Phi_{m'}(g) = \Phi_{m'}(\varphi'(m')) > \Phi_{m'}(\varphi(m')) = \Phi_{m'}(\tilde{g})$, (i.e., $g \succ_{m'} \tilde{g}$). Then, we have $m' \succ_g m$ and $g \succ_{m'} \tilde{g}$ under φ. Thus, (g, m') is a blocking part under φ, contradicting the assumption that φ is stable. □

The convergence and optimality analysis of Algorithm 2 is presented in the following.

Theorem 3 (Local optimality)**.** *Algorithm 2 converges to a local optimal power allocation, PS ratio, and matching solution.*

Proof. From Theorem 1, the convergence of the matching-based algorithm (Algorithm 1) was proved. The convergence of Algorithm 2 also depends on Step 2. Next, we prove the convergence of the iterative procedure in Step 2. We recall that $U(\boldsymbol{\chi}, \boldsymbol{P}, \boldsymbol{\rho}) = \sum_{g=1}^{N} U_g(\boldsymbol{\chi}_g, \boldsymbol{p}_g, \boldsymbol{\rho}_g)$. For each user group g and given $\boldsymbol{\chi}_g$ from the matching-based subchannel assignment algorithm, at iteration t, we have

$$U_g(\boldsymbol{\chi}_g, \boldsymbol{p}_g^{\tau}, \boldsymbol{\rho}_g^{\tau}) \overset{(a)}{\geq} U_g(\boldsymbol{\chi}_g, \boldsymbol{p}_g^{\tau+1}, \boldsymbol{\rho}_g^{\tau}) \overset{(b)}{\geq} U_g(\boldsymbol{\chi}_g, \boldsymbol{p}_g^{\tau+1}, \boldsymbol{\rho}_g^{\tau+1}), \tag{64}$$

where relation (a) is due to $\boldsymbol{p}_g^{\tau+1}$ being the minimizer of U_g for a given $(\boldsymbol{\chi}_g, \boldsymbol{\rho}_g^{\tau})$ and relation (b) is due to $\boldsymbol{\rho}_g^{\tau+1}$ being the minimizer of U_g for a given $(\boldsymbol{\chi}_g, \boldsymbol{p}_g^{\tau})$. Thus, we have $U(\boldsymbol{\chi}, \boldsymbol{p}^{\tau}, \boldsymbol{\rho}^{\tau}) \geq U(\boldsymbol{\chi}, \boldsymbol{p}^{\tau+1}, \boldsymbol{\rho}^{\tau+1})$. This outcome implies that the objective function U is non-increasing after each iteration. Moreover, the lower bound of the utility exists due to the limited resources. Hence, Algorithm 2 is guaranteed to converge. □

2) Performance Analysis of Lyapunov Optimization: We analyze the performance of the proposed algorithm based on the Lyapunov optimization, including the performance gap between the optimal transmit power and the transmit power obtained by the proposed algorithm, the queue stability, and the upper bound of the long-term average data queue length.

Theorem 4. *Suppose that Problem **(P1)** is feasible, $\mathbb{E}\{L(\boldsymbol{\Omega}(0))\} < \infty$ at initial time slot $t = 0$, and $\mathbb{E}\{P_0(t)\} \geq$*

TABLE II
SIMULATION PARAMETERS

Parameter	Value
Bandwidth B	10 MHz
Path loss at distance d with carrier frequency f_c	$PL_{f_c}(d) = 22.7 + 26\log_{10}(f_c) + 36.7\log_{10}(d)$ dB
Battery energy availability threshold θ_i	10 mJ
Maximum battery capacity B_i^{max}	100 mJ
Maximum power budget P_g^{max}	15 dBm
Maximum harvested power at GUE H_k^{max}	20 mW
Non-linear EH circuit specifications (a_k, b_k) [40]	$(150, 0.014)$

$P_{min} > 0$, *where* $P_0(t) = \sum_{g=1}^{N} P_{0,g}(t)$. *Then, we obtain the following:*

(a) The long-term averaged transmit power at the source obtained by solving ***(P2)*** *is upper bounded by the sum of the minimum transmit power* P_0^{opt} *of Problem* ***(P1)*** *and a positive constant, as follows:*

$$\limsup_{T\to\infty} \frac{1}{T}\sum_{t=0}^{T-1} \mathbb{E}\left\{P_0(t)\right\} \leq P_0^{opt} + \frac{\xi}{V}, \tag{65}$$

(b) All queues $Y_i(t), Z_i(t)$, *and* $Q_i(t)$ *are mean rate stable, and Constraints* (21), (22), *and* (25) *are satisfied, respectively.*

(c) The long-term averaged data queue length is upper-bounded by

$$\limsup_{T\to\infty} \frac{1}{T}\sum_{t=0}^{T-1}\sum_{i\in\mathcal{N}} \mathbb{E}\{Q_i(t)\} \leq \frac{\xi + V(P_0^{opt} - P_{min})}{\zeta}. \tag{66}$$

Proof. Please see Appendix E. □

From the above theorem, two observations are further analyzed.

- *Observation 1:* Based on the result in (b), if Problem **(P2)** is feasible and obtains an optimal solution, then all queues are mean rate stable, which immediately implies that the long-term average Constraints (21), (22), and (25) in Problem **(P1)** are all guaranteed. The Constraints (21) and (22) are satisfied due to Lemma 1.
- *Observation 2:* Based on the result in (a), we can design a control algorithm that can ensure nearly-optimal power consumption arbitrarily close to P_0^{opt} by setting a large value for parameter V (i.e., by making $\frac{\xi}{V}$ small). However, according to (c), the bound of the long-term average queue backlog increases linearly in V, leading to the performance-backlog tradeoff of $[\mathcal{O}(\frac{1}{V}), \mathcal{O}(V)]$. This case is further verified in the simulation.

3) Complexity Analysis: The complexity of Algorithm 2 depends on the complexity of the bisection algorithm (for determining the optimal power allocation and PS ratio) and the matching algorithm (Algorithm 1) for subchannel assignment. First, the complexity of the bisection algorithm is $\mathcal{O}\left(\log((R_{up} - R_{lower})/\epsilon)\right)$, where R_{up} and R_{lower} denote the upper and lower bounds for the initial interval, respectively, and ϵ denotes the predefined accuracy. Accordingly, for each user group g, the bisection algorithm for determining p_g^{sum}, ρ_{2g-1} and ρ_{2g} has the complexities of $\mathcal{O}\left(\log(P_g^{max}/\epsilon)\right), \mathcal{O}\left(\log(1/\epsilon)\right)$, and $\mathcal{O}\left(\log(1/\epsilon)\right)$, respectively. Therefore, over N groups, the complexity is $\mathcal{O}\left(N\left[\log(P_g^{max}/\epsilon) + 2\log(1/\epsilon)\right]\right)$. Second, for the subchannel assignment algorithm, the complexities for sorting the preference list of a user group and subchannel are $\mathcal{O}\left(M\log M\right)$ and $\mathcal{O}\left(N\log N\right)$, respectively. The total length of the input preferences in Algorithm 1 is $2NM$. According to [41], the complexity for Algorithm 1 is $\mathcal{O}(NM)$. Then, the total complexity for the Algorithm 2 is $\mathcal{O}\left(N\left[\log(P_g^{max}/\epsilon) + 2\log(1/\epsilon)\right] + NM\right)$. Critically, the joint optimization of power allocation and the PS ratio is performed in a distributed manner for each user group; hence, parallel computing can be used to accelerate the computing process, particularly in large-scale systems.

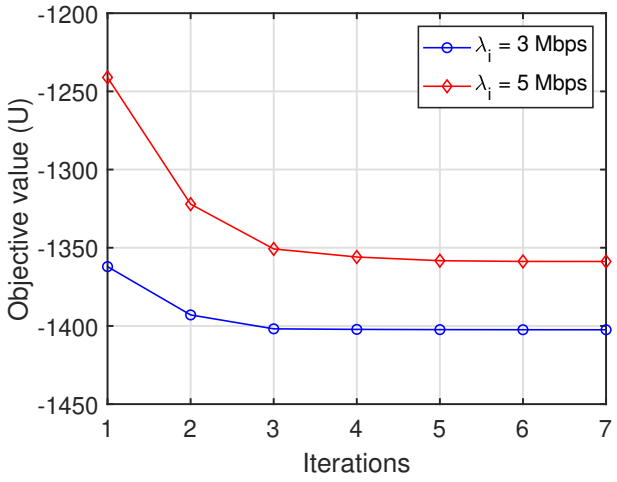

Fig. 3. Convergence behavior of Algorithm 2.

V. Evaluations

A. Simulation Parameters and Comparison Schemes

This section evaluates the proposed scheme in terms of the time average transmit power consumption and achievable rate. We first consider the system of one GBS located at the origin and six GUEs, including three inner and three outer users located inside circles of radii of 10 and 15 m, respectively. They are partitioned into $N = 3$ pairs, each including one inner and one outer user. The total bandwidth $B = 10$

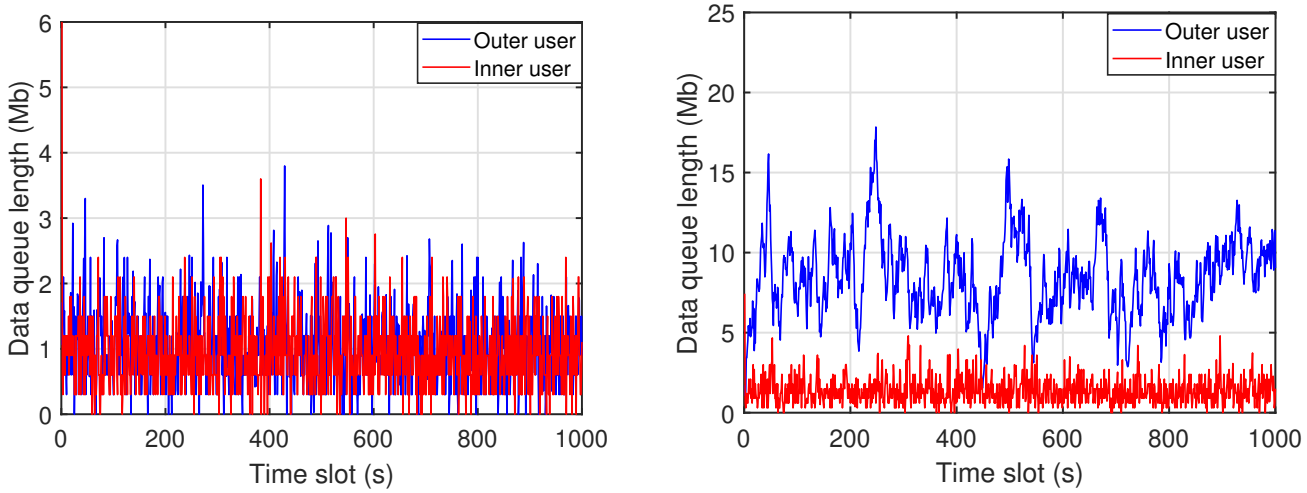

(a) Data queue, $V = 0.1$

(b) Data queue, $V = 5$

Fig. 4. Data queue dynamics versus time.

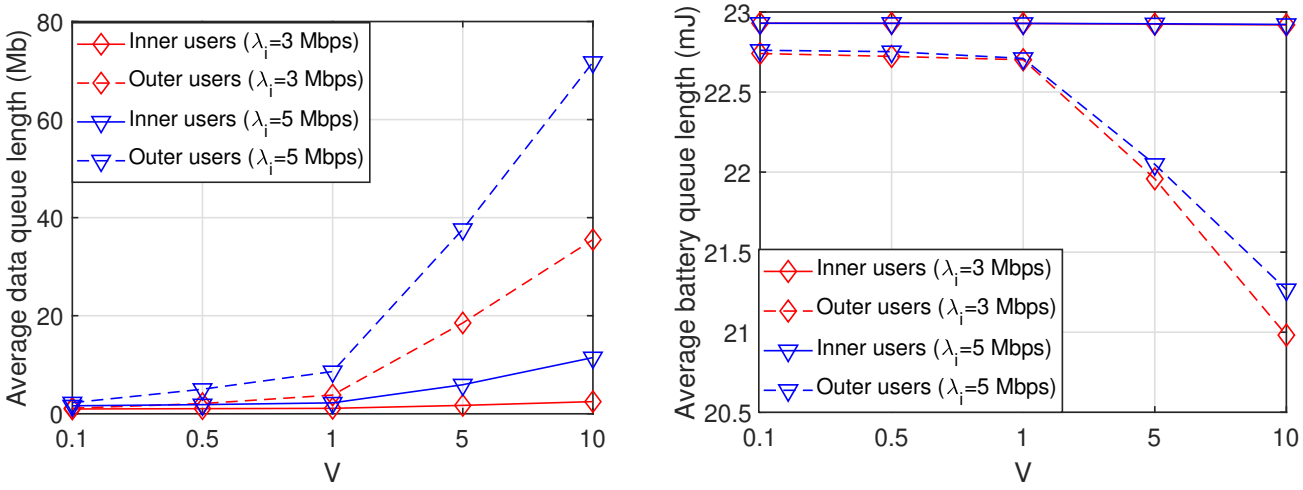

(a) Data queue

(b) Battery queue

Fig. 5. Average data and battery queue length versus the Lyapunov parameter V.

MHz is equally divided into $M = 3$ subchannels so that the bandwidth of each subchannel is $B_c = B/M = 10/3$ MHz. The subchannels for outer and inner users are assumed to undergo Rayleigh and Rician fading, respectively. Simulation parameters were selected according to [42], as summarized in Table II.

To validate the performance of the proposed scheme, we used the following two comparison schemes:

- *OMA-Controlled-SWIPT-Lyapunov:* In this scheme, the total bandwidth is divided into six orthogonal subchannels, each assigned to each user. The proposed Lyapunov optimization method was also applied to determine the solution.
- *OMA-Fixed-SWIPT:* In this scheme, we used the same OFDMA using SWIPT. Here, PS ratio is fixed, and the power allocation at every time slot is determined by setting the service data rate to be the rate of arrived data.

B. Simulation Results

Fig. 3 shows the convergence behavior of the proposed algorithm, with $\lambda_i \in \{3, 5\}$ (Mbps) and U is the value of the objective function in **(P2)**. As can be seen, Algorithm 2 converges after a small number of iterations, which demonstrates the effectiveness of the proposed algorithm.

Fig. 4 shows the data queue dynamics over time under the proposed control scheme. We consider two specific values of the control parameter $V \in \{0.1, 5\}$ with $\lambda_i = 3$ (Mbps) and $P_g^{max} = 15$ (dBm). In Fig. 4(a), for small value V, the system focuses on stabilizing the data queue. Therefore, over time, both queues have small variations and fluctuate around 1 Mb. In contrast, in Fig. 4(b), for a larger value of V, the variation is greater, especially for the outer user's queue, because with a high value of V, the system focuses on minimizing power consumption rather than stabilizing the data queue. As a result, the outer user, allocated with low power, can experience a

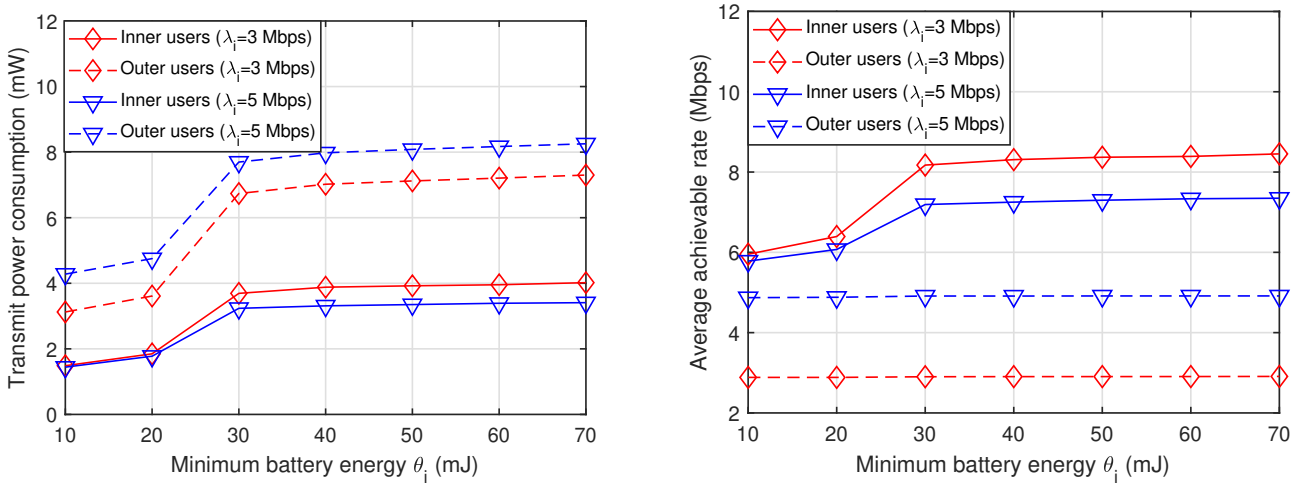

(a) (b)

Fig. 6. Average transmit power consumption and achievable rate versus the minimum energy battery threshold θ_i.

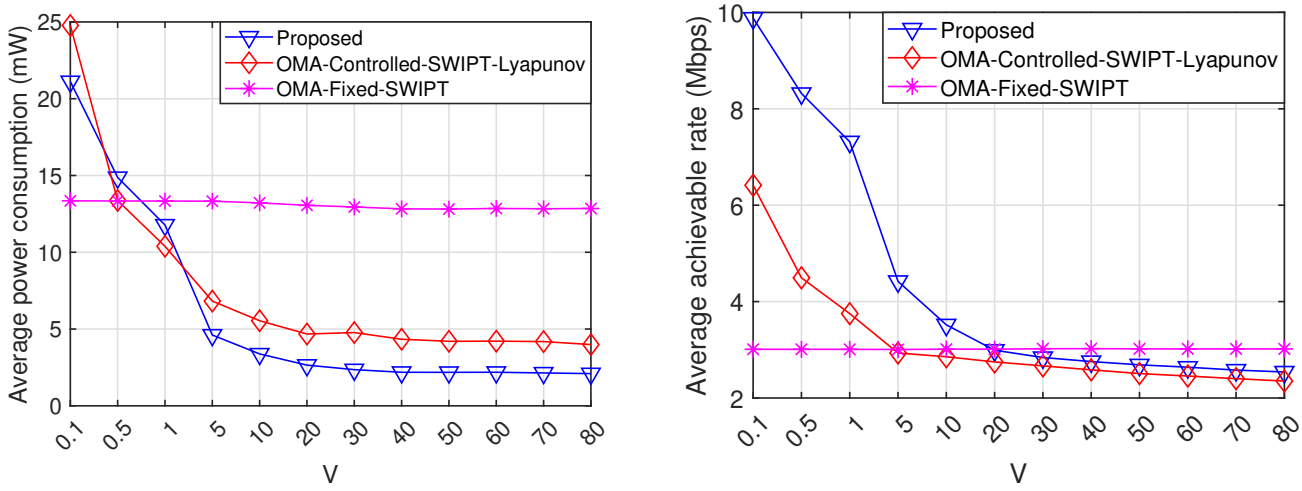

(a) Power consumption (b) Achievable rate

Fig. 7. Average transmit power consumption and achievable rate versus the Lyapunov parameter V.

lower service rate leading to an increase in the queue length over a period.

In Fig. 5(a), the average data queue length w.r.t. V is evaluated under various data arrival rates. We set the values of arrival rate $\lambda_i \in \{3, 5\}$ (Mbps) and $P_g^{max} = 15$ (dBm). The average data queue length of the inner and outer users increases as V increases. This fact matches with Theorem 4 in Section IV-D. Moreover, for the same value of V, a higher arrival rate causes a higher average data queue length. In Fig. 5(b), the average battery queue length w.r.t. V is evaluated under various data arrival rates $\lambda_i \in \{3, 5\}$ (Mbps). The average battery queue length of the inner and outer users decreases as V increases because a higher value of V implies lower allocated power. As a result, lower energy is charged to the users' battery. Moreover, for the same value of V, a higher arrival rate causes a higher average battery queue length.

Fig. 6(a) shows the impact of the minimum battery energy threshold θ_i on the average transmit power consumption with $\lambda_i \in \{3, 5\}$ (Mbps) and $V = 5$. We can observe that the average transmit power consumption for inner and outer users increases as θ_i increases. Fig. 6(b) shows the impact of the minimum battery energy threshold on the average achievable rate. The result reveals that as θ_i increases, the average achievable rate of outer users increases, while that of inner users is constant. With the fixed value of θ_i, the outer users can archive a higher rate, while the inner users lose their achievable rate. This is because as shown in Fig. 6(a), more transmit power should be allocated to outer users to satisfy the minimum battery energy level and data queue stability.

Next, we validate the performance of the proposed algorithm compared with two baseline schemes. In Fig. 7, the average power consumption and achievable rate are evaluated w.r.t. V. We set $\lambda_i = 3$ (Mbps) and $P_g^{max} = 15$ (dBm). Fig. 7(a) reveals that, the average power consumption of

the proposed control and OMA-Controlled-SWIPT-Lyapunov-based control decreases as V increases, whereas that of the OMA-Fixed-SWIPT-based method is constant. This outcome is because the two former methods employ the Lyapunov optimization method to maintain low power consumption with a high value of V, whereas the latter method, which does not rely on the value of V, only allocates power based on the arrival rate to ensure the rate and battery energy requirements. In Fig. 7(b), the achievable rate decreases as V increases, a direct result of decreasing the transmit power consumption from Fig. 7(a). Moreover, in both figures, we can see that the proposed scheme outperforms the two baseline schemes in terms of average transmit power consumption and the achievable rate with a large value of V.

VI. Conclusions

This paper proposes a new resource allocation scheme for SWIPT-NOMA-based GCNs. We first formulated a non-convex problem that minimizes transmit power consumption while supporting the minimum downlink user rate, downlink data queue stability, and user battery queue stability. We transformed the problem into a Lyapunov-drift-penalty minimization problem and decomposed it into the subchannel assignment, power allocation, and PS ratio subproblems. We found the low-complexity solutions to these subproblems and a nearly optimal solution using an AO-based framework and the bisection method. We proved the solution's convergence, optimality, and polynomial computation complexity. Last, through simulations, we demonstrated that the proposed control outperforms benchmark controls regarding transmit power consumption and the achievable rate. Owing to the low-complexity and optimality of proposed solution, the proposed controls can be efficiently applied to large-scale and distributed GCN 6G environments.

Appendix A
Proof of Lemma 1

Proof. According to the update of (27), we have

$$\begin{aligned} &Y_i(t+1)-Y_i(t)\\ &=\begin{cases} R_i^{req}-R_{m,i}(t), & \text{if} \quad Y_i(t)\geq R_{m,i}(t)-R_i^{req}\\ -Y_i(t), & \text{if} \quad Y_i(t)<R_{m,i}(t)-R_i^{req}\end{cases}\\ &\geq R_i^{req}-R_{m,i}(t). \end{aligned} \tag{67}$$

Summing both sides of (67) over $t \in \{0,1,...,T-1\}$, dividing by T, taking the expectation, and letting T go to infinity yields $\lim_{T\to\infty}\frac{\mathbb{E}\{Y_i(T)\}}{T} \geq R_i^{req} - \lim_{T\to\infty}\frac{1}{T}\sum_{t=0}^{T-1}\mathbb{E}\{R_i(t)\}$. If the virtual queue $Y_i(t)$ is mean rate stable, i.e., $\lim_{T\to\infty}\frac{\mathbb{E}\{Y_i(T)\}}{T}=0$, we have $\lim_{T\to\infty}\frac{1}{T}\sum_{t=0}^{T-1}\mathbb{E}\{R_i(t)\}\geq R_i^{req}$. The same arguments can be made for the virtual queue Z_i, which completes the proof. □

Appendix B
Proof of Lemma 2

Proof. Squaring the update equations in (15), (19), (27), and (28), and applying the inequality $\max\{a-b,0\}^2\leq(a-b)^2$ yields

$$\begin{aligned}\frac{Q_i^2(t+1)-Q_i^2(t)}{2} &\leq \frac{R_{m,i}^2(t)+A_i^2(t)}{2}\\ &\quad+Q_i(t)\left[A_i(t)-R_{m,i}(t)\right],\end{aligned} \tag{68}$$

$$\begin{aligned}&\frac{[B_i^{max}-B_i(t+1)]^2-[B_i^{max}-B_i(t)]^2}{2}\leq\\ &\frac{C_i(t)^2+(EH_{m,i}(t))^2}{2}+[B_i^{max}-B_i(t)][C_i(t)-EH_{m,i}(t)],\end{aligned} \tag{69}$$

$$\begin{aligned}\frac{Y_i^2(t+1)-Y_i^2(t)}{2} &\leq \frac{(R_i^{req})^2+R_{m,i}^2(t)}{2}\\ &\quad+Y_i(t)\left[R_i^{req}-R_{m,i}(t)\right],\end{aligned} \tag{70}$$

$$\begin{aligned}\frac{Z_i^2(t+1)-Z_i^2(t)}{2} &\leq B_i(t)^2+(\mathrm{EH}_{m,i}(t))^2+\frac{\theta_i^2}{2}\\ &\quad+Z_i(t)[\theta_i-D_i(t)].\end{aligned} \tag{71}$$

Combining the inequalities from (68) to (71), we can obtain the upper bound in (32) with constant β specified in (32). This statement completes the proof. □

Appendix C
Proof of Lemma 3

Proof. Taking the first-order derivative of $F(p_{m,2g})$ with respect to (w.r.t.) $p_{m,2g}$ yields $F'(p_{m,2g}) = (\alpha_{2g-1}-\alpha_{2g})\,\rho_{2g-1}\rho_{2g}$. Thus, if $(\alpha_{2g-1}-\alpha_{2g})\rho_{2g-1}\rho_{2g}>0$ then $F'(p_{m,2g})>0$ (i.e., $F(p_{m,2g})$ is strictly increasing on $\left[0,p_g^{sum}/2\right]$). Moreover, if $(\alpha_{2g-1}-\alpha_{2g})\rho_{2g-1}\rho_{2g}=0$, then $F(p_{m,2g})=\alpha_{2g-1}\rho_{2g-1}\nu_{m,2g}-\alpha_{2g}\rho_{2g}\nu_{m,2g-1}$, which is a constant. Otherwise, it is strictly decreasing. □

Appendix D
Proof of Lemma 4

Proof. Computing the second-order derivative of $f_s(p_g^{sum})$ w.r.t. p_g^{sum} yields

$$\begin{aligned} &f_s{}''(p_g^{sum})\\ &=\frac{\alpha_{2g-1}\rho_{2g-1}^2}{\log(2)\left(\rho_{2g-1}p_g^{sum}+\nu_{m,2g-1}\right)^2}\\ &\quad+\frac{\left[\begin{array}{r}\eta_{m,2g-1}^2\beta_{2g-1}B_{2g-1}H_{2g-1}^{max}e^{-\eta_{m,2g-1}p_g^{sum}-\xi_{2g-1}}\\ \times\left(1-e^{-\eta_{m,2g-1}p_g^{sum}-\xi_{2g-1}}\right)\end{array}\right]}{\left(1+e^{-\eta_{m,2g-1}p_g^{sum}-\xi_{2g-1}}\right)^3}\\ &\quad+\frac{\left[\begin{array}{r}\eta_{m,2g}^2\beta_{2g}B_{2g}H_{2g}^{max}e^{-\eta_{m,2g}p_g^{sum}-\xi_{2g}}\\ \times\left(1-e^{-\eta_{m,2g}p_g^{sum}-\xi_{2g}}\right)\end{array}\right]}{\left(1+e^{-\eta_{m,2g}p_g^{sum}-\xi_{2g}}\right)^3}\end{aligned} \tag{72}$$

From the second term of (72), we can see that $1-e^{-\eta_{m,2g-1}p_g^{sum}-\xi_{2g-1}}\geq 0$ if $P_{m,2g-1}^{EH}\geq b_{2g-1}$, and $1-e^{-\eta_{m,2g-1}p_g^{sum}-\xi_{2g-1}}<0$, otherwise. The second case cannot be used since $P_{m,2g-1}^{EH}$ is so small that satisfy the minimum battery energy requirement. We also have a similar result for the last term of (72). Therefore, we can conclude that $f_s{}''(p_g^{sum})\geq 0$, i.e., $f_s(p_g^{sum})$ is convex. □

APPENDIX E
PROOF OF THEOREM 4

Before proving this theorem, we first provide a related lemma.

Lemma 6. *[33], [43] Suppose that a point $\boldsymbol{\lambda} = \{\lambda_i\}_{i\in\mathcal{N}}$ is strictly interior to capacity region Λ[1], and $\boldsymbol{\lambda}+\zeta$ is still in Λ for a $\zeta > 0$. If Problem **(P1)** is feasible, then for any $\kappa > 0$, a stationary randomized policy $(\boldsymbol{\chi}^*(t), \boldsymbol{P}^*(t), \boldsymbol{\rho}^*(t))$ exists that is independent of the queues, such that*

$$\begin{aligned}&\mathbb{E}\left\{P_0^*(t)|\boldsymbol{\Omega}(t)\right\} = \mathbb{E}\left\{P_0^*(t)\right\} \le P_0^{opt} + \kappa,\\ &\mathbb{E}\{R_{m,i}^*(t)|\boldsymbol{\Omega}(t)\} = \mathbb{E}\{R_{m,i}^*(t)\} \ge \mathbb{E}\{A_i^*(t)\} + \zeta,\end{aligned} \tag{73}$$

$$\begin{aligned}&\mathbb{E}\left\{R_i^{req} - R_{m,i}^*(t)|\boldsymbol{\Omega}(t)\right\} = \mathbb{E}\left\{R_i^{req} - R_{m,i}^*(t)\right\} \le \kappa,\\ &\mathbb{E}\left\{\theta_i - D_i^*(t)|\boldsymbol{\Omega}(t)\right\} = \mathbb{E}\left\{\theta_i - D_i^*(t)\right\} \le \kappa,\end{aligned} \tag{74}$$

where $P_0^*(t)$, $A_i^*(t), R_{m,i}^*(t)$, and $D_i^*(t)$ are the resulting values under the policy.

Applying this lemma, we can prove the theorem as follows.
(a) From Lemma 6, we consider the policy $(\boldsymbol{\chi}^*(t), \boldsymbol{P}^*(t), \boldsymbol{\rho}^*(t))$ that satisfies (73)-(74). Then, substituting these inequalities into the right-hand-side of (32) and taking $\kappa \to 0$ yields

$$\begin{aligned}\Delta(\boldsymbol{\Omega}(t)) + V\mathbb{E}\left\{P_0(t)|\boldsymbol{\Omega}(t)\right\} &\le \xi + VP_0^{opt} - \zeta\sum_{i\in\mathcal{N}} w_{1,i}Q_i(t)\\ &\le \xi + VP_0^{opt}.\end{aligned} \tag{75}$$

Taking expectation and summing over $t \in \{0, 2, ..., T-1\}$ yields

$$\begin{aligned}&\mathbb{E}\left\{L(\boldsymbol{\Omega}(T))\right\} - \mathbb{E}\left\{L(\boldsymbol{\Omega}(0))\right\} + V\sum_{t=0}^{T-1}\mathbb{E}\left\{P_0(t)\right\}\\ &\qquad\le T\left(\xi + VP_0^{opt}\right).\end{aligned} \tag{76}$$

By rearranging and dividing both sides of the above inequality by TV, and letting $T \to \infty$, we obtain (65).

(b) We first demonstrate that $\lim_{T\to\infty}\frac{\mathbb{E}\{Q_i(T)\}}{T} = 0$ and similarly, for $Y_i(t)$ and $Z_i(t)$. From (76), neglecting the non-negative term $V\sum_{t=0}^{T-1}\mathbb{E}\left\{P_0(t)\right\}$ yields

$$\mathbb{E}\left\{L(\boldsymbol{\Omega}(T))\right\} \le T\left(\xi + VP_0^{opt}\right) + \mathbb{E}\left\{L(\boldsymbol{\Omega}(0))\right\}. \tag{77}$$

By the definition of $L(\boldsymbol{\Omega}(t))$ in (29) and because $\mathbb{E}\{Q_i^2(t)\} \ge \mathbb{E}\{Q_i(t)\}^2$, we have

$$\frac{w_{1,i}}{2}\mathbb{E}\left\{Q_i(T)\right\}^2 \le T\left(\xi + VP_0^{opt}\right) + \mathbb{E}\left\{L(\boldsymbol{\Omega}(0))\right\}. \tag{78}$$

Taking the square root and dividing both sides of the above inequality by T yields

$$\frac{\mathbb{E}\left\{Q_i(T)\right\}}{T} \le \frac{1}{T}\sqrt{\frac{2T\left(\xi + VP_0^{opt}\right) + 2\mathbb{E}\left\{L(\boldsymbol{\Omega}(0))\right\}}{w_{1,i}}}. \tag{79}$$

With $T \to \infty$ and $0 < w_{1,i} < \infty$, we obtain $\lim_{T\to\infty}\frac{\mathbb{E}\{Q_i(T)\}}{T} = 0$ because $\mathbb{E}\left\{L(\boldsymbol{\Omega}(0))\right\} < \infty$.

(c) From the first inequality in (75), taking the iterated expectation and applying telescoping sums over $t \in \{0, 1, \ldots, T-1\}$ for some $T > 0$ [33], we obtain the following:

$$\begin{aligned}&\mathbb{E}\left\{L(\boldsymbol{\Omega}(T))\right\} - \mathbb{E}\left\{L(\boldsymbol{\Omega}(0))\right\} + V\sum_{t=0}^{T-1}\mathbb{E}\left\{P_0(t)\right\}\\ &\qquad\le T\left(\xi + VP_0^{opt}\right) - \zeta\sum_{t=0}^{T-1}\sum_{i\in\mathcal{N}}\mathbb{E}\{Q_i(t)\}.\end{aligned}$$

Dividing both sides by ζT, where $T \to \infty$, we have

$$\limsup_{T\to\infty}\frac{1}{T}\sum_{t=0}^{T-1}\sum_{i\in\mathcal{N}}\mathbb{E}\{Q_i(t)\} \le \frac{\xi + V(P_0^{opt} - P_{min})}{\zeta}. \tag{80}$$

[1]The capacity region is defined as all data arrival rates, which ensures the existence of a policy that stabilizes the networks [43], [44].

REFERENCES

[1] T. Huang, W. Yang, J. Wu, J. Ma, X. Zhang, and D. Zhang, "A survey on green 6G network: Architecture and technologies," *IEEE Access*, vol. 7, pp. 175 758–175 768, 2019.

[2] L. Liu, C. Yuen, Y. L. Guan, Y. Li, and C. Huang, "Gaussian message passing for overloaded massive MIMO-NOMA," *IEEE Transactions on Wireless Communications*, vol. 18, no. 1, pp. 210–226, 2019.

[3] T. D. P. Perera, D. N. K. Jayakody, S. K. Sharma, S. Chatzinotas, and J. Li, "Simultaneous wireless information and power transfer (SWIPT): Recent advances and future challenges," *IEEE Communications Surveys & Tutorials*, vol. 20, no. 1, pp. 264–302, 2017.

[4] S. Mao, S. Leng, J. Hu, and K. Yang, "Power minimization resource allocation for underlay MISO-NOMA SWIPT systems," *IEEE Access*, vol. 7, pp. 17 247–17 255, 2019.

[5] Z. Song, X. Wang, Y. Liu, and Z. Zhang, "Joint spectrum resource allocation in NOMA-based cognitive radio network with SWIPT," *IEEE access*, vol. 7, pp. 89 594–89 603, 2019.

[6] J. Tang, J. Luo, M. Liu, D. K. So, E. Alsusa, G. Chen, K.-K. Wong, and J. A. Chambers, "Energy efficiency optimization for NOMA with SWIPT," *IEEE Journal of Selected Topics in Signal Processing*, vol. 13, no. 3, pp. 452–466, 2019.

[7] J. Tang, J. Luo, J. Ou, X. Zhang, N. Zhao, D. K. C. So, and K.-K. Wong, "Decoupling or learning: Joint power splitting and allocation in MC-NOMA with SWIPT," *IEEE Transactions on Communications*, vol. 68, no. 9, pp. 5834–5848, 2020.

[8] A. Andrawes, R. Nordin, and N. F. Abdullah, "Energy-efficient downlink for non-orthogonal multiple access with SWIPT under constrained throughput," *energies*, vol. 13, no. 1, p. 107, 2019.

[9] P. D. Diamantoulakis and G. K. Karagiannidis, "Maximizing proportional fairness in wireless powered communications," *IEEE Wireless Communications Letters*, vol. 6, no. 2, pp. 202–205, 2017.

[10] Z. Yang, Z. Ding, P. Fan, and N. Al-Dhahir, "The impact of power allocation on cooperative non-orthogonal multiple access networks with SWIPT," *IEEE Transactions on Wireless Communications*, vol. 16, no. 7, pp. 4332–4343, 2017.

[11] Y. Liu, Z. Ding, M. Elkashlan, and H. V. Poor, "Cooperative non-orthogonal multiple access with simultaneous wireless information and power transfer," *IEEE Journal on Selected Areas in Communications*, vol. 34, no. 4, pp. 938–953, 2016.

[12] M. Alageli, A. Ikhlef, and J. Chambers, "Optimization for maximizing sum secrecy rate in MU-MISO SWIPT systems," *IEEE Transactions on Vehicular Technology*, vol. 67, no. 1, pp. 537–553, 2017.

[13] Y. Liu, Z. Ding, M. Elkashlan, and H. V. Poor, "Cooperative non-orthogonal multiple access with simultaneous wireless information and power transfer," *IEEE Journal on Selected Areas in Communications*, vol. 34, no. 4, pp. 938–953, 2016.

[14] T. N. Do, D. B. da Costa, T. Q. Duong, and B. An, "Improving the performance of cell-edge users in MISO-NOMA systems using TAS and SWIPT-based cooperative transmissions," *IEEE Transactions on Green Communications and Networking*, vol. 2, no. 1, pp. 49–62, 2017.

[15] R. R. Kurup and A. Babu, "Power adaptation for improving the performance of time switching SWIPT-based full-duplex cooperative NOMA network," *IEEE Communications Letters*, vol. 24, no. 12, pp. 2956–2960, 2020.

[16] C. Guo, L. Zhao, C. Feng, Z. Ding, and H.-H. Chen, "Energy harvesting enabled NOMA systems with full-duplex relaying," *IEEE Transactions on Vehicular Technology*, vol. 68, no. 7, pp. 7179–7183, 2019.

[17] X. Li, J. Li, and L. Li, "Performance analysis of impaired SWIPT-NOMA relaying networks over imperfect Weibull channels," *IEEE Systems Journal*, vol. 14, no. 1, pp. 669–672, 2019.

[18] A. Celik, M.-C. Tsai, R. M. Radaydeh, F. S. Al-Qahtani, and M.-S. Alouini, "Distributed user clustering and resource allocation for imperfect NOMA in heterogeneous networks," *IEEE Transactions on Communications*, vol. 67, no. 10, pp. 7211–7227, 2019.

[19] J. Guo, J. Lu, X. Wang, and L. Zhou, "Performance analysis of SWIPT-assisted adaptive NOMA/OMA system with hardware impairments and imperfect CSI," *ETRI Journal*, 2022.

[20] J. Zhou, Y. Sun, Q. Cao, S. Li, H. Xu, and W. Shi, "QoS-based robust power optimization for SWIPT-NOMA system with statistical CSI," *IEEE Transactions on Green Communications and Networking*, vol. 3, no. 3, pp. 765–773, 2019.

[21] Y. Xu, Z. Liu, Z. Yang, and C. Huang, "Energy-efficient resource allocation with imperfect CSI in NOMA-based D2D networks with SWIPT," in *2021 IEEE Wireless Communications and Networking Conference (WCNC)*, 2021, pp. 1–6.

[22] B. Xia, Y. Fan, J. Thompson, and H. V. Poor, "Buffering in a three-node relay network," *IEEE Transactions on Wireless Communications*, vol. 7, no. 11, pp. 4492–4496, 2008.

[23] N. Zlatanov, R. Schober, and P. Popovski, "Buffer-aided relaying with adaptive link selection," *IEEE Journal on Selected Areas in Communications*, vol. 31, no. 8, pp. 1530–1542, 2012.

[24] J. Ren, X. Lei, F. Zhou, P. D. Diamantoulakis, O. A. Dobre, and G. K. Karagiannidis, "Throughput maximization in buffer-aided wireless-powered NOMA networks," in *ICC 2020-2020 IEEE International Conference on Communications (ICC)*. IEEE, 2020, pp. 1–7.

[25] X. Lan, Y. Zhang, Q. Chen, and L. Cai, "Energy efficient buffer-aided transmission scheme in wireless powered cooperative NOMA relay network," *IEEE Transactions on Communications*, vol. 68, no. 3, pp. 1432–1447, 2019.

[26] Y. Saito, Y. Kishiyama, A. Benjebbour, T. Nakamura, A. Li, and K. Higuchi, "Non-orthogonal multiple access (NOMA) for cellular future radio access," in *Proc. IEEE 77th vehicular technology conference (VTC Spring)*, 2013, pp. 1–5.

[27] Z. Ding, P. Fan, and H. V. Poor, "Impact of user pairing on 5G non-orthogonal multiple-access downlink transmissions," *IEEE Transactions on Vehicular Technology*, vol. 65, no. 8, pp. 6010–6023, 2015.

[28] J. Tang, J. Luo, J. Ou, X. Zhang, N. Zhao, D. K. C. So, and K.-K. Wong, "Decoupling or learning: joint power splitting and allocation in MC-NOMA with SWIPT," *IEEE Transactions on Communications*, vol. 68, no. 9, pp. 5834–5848, 2020.

[29] J. Zhao, Y. Liu, K. K. Chai, A. Nallanathan, Y. Chen, and Z. Han, "Spectrum allocation and power control for non-orthogonal multiple access in HetNets," *IEEE Transactions on Wireless Communications*, vol. 16, no. 9, pp. 5825–5837, 2017.

[30] M. F. Hanif, Z. Ding, T. Ratnarajah, and G. K. Karagiannidis, "A minorization-maximization method for optimizing sum rate in the downlink of non-orthogonal multiple access systems," *IEEE Transactions on Signal Processing*, vol. 64, no. 1, pp. 76–88, 2015.

[31] C. R. Valenta and G. D. Durgin, "Harvesting wireless power: Survey of energy-harvester conversion efficiency in far-field, wireless power transfer systems," *IEEE Microwave Magazine*, vol. 15, no. 4, pp. 108–120, 2014.

[32] E. Boshkovska, D. W. K. Ng, N. Zlatanov, and R. Schober, "Practical non-linear energy harvesting model and resource allocation for SWIPT systems," *IEEE Communications Letters*, vol. 19, no. 12, pp. 2082–2085, 2015.

[33] M. J. Neely, "Stochastic network optimization with application to communication and queueing systems," *Synthesis Lectures on Communication Networks*, vol. 3, no. 1, pp. 1–211, 2010.

[34] Y. Gu, W. Saad, M. Bennis, M. Debbah, and Z. Han, "Matching theory for future wireless networks: Fundamentals and applications," *IEEE Communications Magazine*, vol. 53, no. 5, pp. 52–59, 2015.

[35] A. E. Roth and M. Sotomayor, *Two-Sided Matching: A Study in Game Theoretic Modeling and Analysis*. Cambridge University Press, 1992.

[36] B. Di, L. Song, and Y. Li, "Sub-channel assignment, power allocation, and user scheduling for non-orthogonal multiple access networks," *IEEE Transactions on Wireless Communications*, vol. 15, no. 11, pp. 7686–7698, 2016.

[37] J. Zuo, Y. Liu, Z. Qin, and N. Al-Dhahir, "Resource allocation in intelligent reflecting surface assisted noma systems," *IEEE Transactions on Communications*, vol. 68, no. 11, pp. 7170–7183, 2020.

[38] T. M. Ho, N. H. Tran, L. B. Le, Z. Han, S. A. Kazmi, and C. S. Hong, "Network virtualization with energy efficiency optimization for wireless heterogeneous networks," *IEEE Transactions on Mobile Computing*, vol. 18, no. 10, pp. 2386–2400, 2018.

[39] E. A. Jorswieck, "Stable matchings for resource allocation in wireless networks," in *Proc. IEEE 17th International Conference on Digital Signal Processing (DSP)*, 2011, pp. 1–8.

[40] D. Kim, M. Choi, and D.-W. Seo, "Energy-efficient power control for simultaneous wireless information and power transfer–nonorthogonal multiple access in distributed antenna systems," *IEEE Transactions on Industrial Informatics*, 2022.

[41] Z. Zhou, K. Ota, M. Dong, and C. Xu, "Energy-efficient matching for resource allocation in D2D enabled cellular networks," *IEEE Transactions on Vehicular Technology*, vol. 66, no. 6, pp. 5256–5268, 2016.

[42] V.-D. Nguyen and O.-S. Shin, "An efficient design for NOMA-assisted MISO-SWIPT systems with AC computing," *IEEE Access*, vol. 7, pp. 97 094–97 105, 2019.

[43] Y. Li, M. Sheng, Y. Shi, X. Ma, and W. Jiao, "Energy efficiency and delay tradeoff for time-varying and interference-free wireless networks," *IEEE Transactions on Wireless Communications*, vol. 13, no. 11, pp. 5921–5931, 2014.

[44] M. J. Neely, "Energy optimal control for time-varying wireless networks," *IEEE transactions on Information Theory*, vol. 52, no. 7, pp. 2915–2934, 2006.

Thi My Tuyen Nguyen received the B.S. degree in Mathematics from University of Science, Ho Chi Minh City, Viet Nam in 2016, and M.S. degree in Computer Science and Engineering from Soongsil University, South Korea in 2021. She is currently pursuing Ph.D. in Big Data at Chung-Ang University, South Korea. Her research interests include machine learning, optimization, and their applications in wireless communications.

The Vi Nguyen received the B.S. degree in Mathematics from University of Science, Ho Chi Minh City, Viet Nam in 2016, and M.S. degree in Computer Science and Engineering from Chung-Ang University, South Korea in 2021. He is currently pursuing Ph.D. in Big Data at Chung-Ang University, South Korea. His research interests include machine learning, optimization, and their applications in wireless communications.

Wonjong Noh received the B.S., M.S., and Ph.D. degrees from the Department of Electronics Engineering, Korea University, Seoul, South Korea, in 1998, 2000, and 2005, respectively. From 2005 to 2007, he conducted the Postdoctoral Research with Purdue University, West Lafayette, IN, USA, and the University of California at Irvine, Irvine, CA, USA. From 2008 to 2015, he was a Principal Research Engineer with the Samsung Advanced Institute of Technology, Samsung Electronics, South Korea. After that, he worked as an Assistant Professor with the Department of Electronics and Communication Engineering, Gyeonggi University of Science and Technology, South Korea, and since 2019, he is working as an Associate Professor with the School of Software, Hallym University, South Korea. He received the Government Postdoctoral Fellowship from the Ministry of Information and Communication, South Korea, in 2005. He was also a recipient of the Samsung Best Paper Gold Award in 2010, the Samsung Patent Bronze Award in 2011, and the Samsung Technology Award in 2013. His current research interests include fundamental analysis and evaluations on machine learning-based 5G and 6G wireless communications and networks.

Sungrae Cho received B.S. and M.S. degrees in Electronics Engineering from Korea University, Seoul, South Korea, in 1992 and 1994, respectively, and Ph.D. degree in Electrical and Computer Engineering from the Georgia Institute of Technology, Atlanta, GA, USA, in 2002. He is a Professor with the School of Computer Science and Engineering, Chung-Ang University (CAU), Seoul, South Korea. Prior to joining CAU, he was an Assistant Professor with the Department of Computer Sciences, Georgia Southern University, Statesboro, GA, USA, from 2003 to 2006, and a Senior Member of Technical Staff with the Samsung Advanced Institute of Technology (SAIT), Kiheung, South Korea, in 2003. From 1994 to 1996, he was a Research Staff Member with Electronics and Telecommunications Research Institute (ETRI), Daejeon, South Korea. From 2012 to 2013, he held a Visiting Professorship with the National Institute of Standards and Technology (NIST), Gaithersburg, MD, USA. His current research interests include wireless networking, ubiquitous computing, and ICT convergence. He has been a Subject Editor of IET Electronics Letter since 2018, and was an Area Editor of Ad Hoc Networks Journal (Elsevier) from 2012 to 2017. He has served numerous international conferences as an Organizing Committee Chair, such as IEEE ICC, SECON, ICOIN, ICTC, ICUFN, TridentCom, and the IEEE MASS, and as a Program Committee Member, such as IEEE ICC, GLOBECOM, VTC, MobiApps, SENSORNETS, and WINSYS.